Research Square

Preprints are preliminary reports that have not undergone peer review.
They should not be considered conclusive, used to inform clinical practice,
or referenced by the media as validated information.

Lifetime perceived thermal stress impacts brain and behavior in healthy young adults.

Chunshui Yu

chunshuiyu@tmu.edu.cn

Tianjin Medical University General Hospital https://orcid.org/0000-0001-5648-5199

Yuan Ji

Department of Radiology, Tianjin Key Lab of Functional Imaging and State Key Laboratory of Experimental Hematology, Tianjin Medical University General Hospital https://orcid.org/0000-0003-2874-5904

Caihong Wang

Department of Magnetic Resonance Imaging, The First Affiliated Hospital of Zhengzhou University

Xiaojun Xu

Department of Radiology, The Second Affiliated Hospital of Zhejiang University, School of Medicine

Zhihan Yan

Department of Radiology, The Second Affiliated Hospital and Yuying Children's Hospital of Wenzhou Medical University

Meiyun Wang

Department of Radiology, Henan Provincial People's Hospital & Zhengzhou University People's Hospital

Long Jiang Zhang

Jinling Hospital, Affiliated Hospital of Medical School, Nanjing University https://orcid.org/0000-0002-6664-7224

Zuojun Geng

Department of Medical Imaging, The Second Hospital of Hebei Medical University

Yongqiang Yu

Department of Radiology, The First Affiliated Hospital of Anhui Medical University

Weihua Liao

Department of Radiology, Xiangya Hospital, Central South University

Hui Zhang

Department of Radiology, The First Hospital of Shanxi Medical University

Bo Gao

Department of Radiology, The Affiliated Hospital of Guizhou Medical University

Tong Han

Department of Radiology, Tianjin Huanhu Hospital

Zhenwei Yao

Department of Radiology, Huashan Hospital, Fudan University

Quan Zhang

Department of Radiology, Characteristic Medical Center of Chinese People's Armed Police Force

Meng Liang

School of Medical Imaging and Tianjin Key Laboratory of Functional Imaging, Tianjin Medical University

Wen Qin

Department of Radiology, Tianjin Key Lab of Functional Imaging and State Key Laboratory of Experimental Hematology, Tianjin Medical University General Hospital

Feng Liu

Tianjin Medical University General Hospital https://orcid.org/0000-0002-3570-4222

Qiang Xu

Department of Radiology, Tianjin Key Lab of Functional Imaging and State Key Laboratory of Experimental Hematology, Tianjin Medical University General Hospital

Jiayuan Xu

Department of Radiology, Tianjin Key Lab of Functional Imaging and State Key Laboratory of Experimental Hematology, Tianjin Medical University General Hospital

Nana Liu

Department of Radiology, Tianjin Key Lab of Functional Imaging and State Key Laboratory of Experimental Hematology, Tianjin Medical University General Hospital

Jie Tang

Department of Radiology, Tianjin Key Lab of Functional Imaging and State Key Laboratory of Experimental Hematology, Tianjin Medical University General Hospital

Sijia Wang

Department of Radiology, Tianjin Key Lab of Functional Imaging and State Key Laboratory of Experimental Hematology, Tianjin Medical University General Hospital

Xue Hui

Department of Radiology, Tianjin Key Lab of Functional Imaging and State Key Laboratory of Experimental Hematology, Tianjin Medical University General Hospital

Haiyan Li

Department of Radiology, Tianjin Key Lab of Functional Imaging and State Key Laboratory of Experimental Hematology, Tianjin Medical University General Hospital

Shuqi Yang

Department of Radiology, Tianjin Key Lab of Functional Imaging and State Key Laboratory of Experimental Hematology, Tianjin Medical University General Hospital

Zhaoxiang Ye

Department of Radiology, Tianjin Medical University Cancer Institute & Hospital, National Clinical Research Center for Cancer, Tianjin’s Clinical Research Center

Peng Zhang

Department of Radiology, Tianjin Medical University Cancer Institute & Hospital, National Clinical Research Center for Cancer, Tianjin's Clinical Research Center

Wei Li

Department of Radiology, Tianjin Medical University Cancer Institute & Hospital, National Clinical Research Center for Cancer, Tianjin's Clinical Research Center

Wei Wei

Department of Radiology, Henan Provincial People's Hospital & Zhengzhou University People's Hospital

Dapeng Shi

Department of Radiology, Henan Provincial People's Hospital & Zhengzhou University People's Hospital

Su Lui

Department of Radiology, Huaxi MR Research Center (HMRRC), Functional and Molecular Imaging key Laboratory of Sichuan Province, West China Hospital of Sichuan University

Feng Chen

Department of Radiology, Hainan General Hospital (Hainan Affiliated Hospital of Hainan Medical University)

Jing Zhang

Department of Magnetic Resonance, Lanzhou University Second Hospital

Wen Shen

Department of Radiology, Tianjin First Center Hospital

Yanwei Miao

Department of Radiology, The First Affiliated Hospital of Dalian Medical University

Dawei Wang

Department of Radiology, Qilu Hospital of Shandong University

Jia-Hong Gao

Center for MRI Research, Academy for Advanced Interdisciplinary Studies, Peking University

Yunjun Yang

Department of Radiology, The First Affiliated Hospital of Wenzhou Medical University

Junfang Xian

Department of Radiology, Beijing Tongren Hospital, Capital Medical University

Wenzhen Zhu

Department of Radiology, Tongji Hospital, Tongji Medical College, Huazhong University of Science and Technology

Kai Xu

Department of Radiology, The Affiliated Hospital of Xuzhou Medical University

Bing Zhang

Department of Radiology, Drum Tower Hospital, Medical School of Nanjing University

Xiaochu Zhang

Division of Life Science and Medicine, University of Science & Technology of China

Shijun Qiu

Department of Radiology, The First Affiliated Hospital of Guangzhou University of Chinese Medicine, Guangzhou

Guangbin Cui

Functional and Molecular Imaging Key Lab of Shaanxi Province & Department of Radiology, Tangdu Hospital, Air Force Medical University

Xi-Nian Zuo

Beijing Normal University https://orcid.org/0000-0001-9110-585X

the CHIMGEN Consortium the CHIMGEN Consortium

Tianjin Medical University General Hospital

Article

Keywords:

Posted Date: August 4th, 2026

DOI: https://doi.org/10.21203/rs.3.rs-10513999/v1

License: This work is licensed under a Creative Commons Attribution 4.0 International License. Read Full License

Additional Declarations: There is **NO** Competing Interest.

Title: Lifetime perceived thermal stress impacts brain and behavior in healthy young adults

Authors list

Yuan Ji[1,41], Caihong Wang[2,41], Xiaojun Xu[3,41], Zhihan Yan[4,41], Meiyun Wang[5,6], Longjiang Zhang[7], Zuojun Geng[8], Yongqiang Yu[9], Weihua Liao[10,11,12], Hui Zhang[13], Bo Gao[14,15], Tong Han[16], Zhenwei Yao[17], Quan Zhang[18], Meng Liang[19], Wen Qin[1], Feng Liu[1], Qiang Xu[1], Jiayuan Xu[1], Nana Liu[1], Jie Tang [1], Sijia Wang[1], Hui Xue[1], Haiyan Li[1], Shuqi Yang[1], Zhaoxiang Ye[20], Peng Zhang[20], Wei Li[20], Wei Wei[5], Dapeng Shi[5], Su Lui[21,22], Feng Chen[23], Jing Zhang[24,25], Wen Shen[26], Yanwei Miao[27], Dawei Wang[28], Jia-Hong Gao[29], Yunjun Yang[30], Junfang Xian[31], Wenzhen Zhu [32], Kai Xu[33], Bing Zhang[34], Xiaochu Zhang[35], Shijun Qiu[36,37#], Guangbin Cui[38#], Xi-Nian Zuo[39,40#], Chunshui Yu[1,19#] and the CHIMGEN Consortium

Affiliations

[1]Department of Radiology, Tianjin Key Lab of Functional Imaging and State Key Laboratory of Experimental Hematology, Tianjin Medical University General Hospital, Tianjin 300052, China.

[2]Department of Magnetic Resonance Imaging, The First Affiliated Hospital of Zhengzhou University, 450052 Zhengzhou, China.

[3]Department of Radiology, The Second Affiliated Hospital of Zhejiang University, School of Medicine, 310009 Hangzhou, China.

[4]Department of Radiology, The Second Affiliated Hospital and Yuying Children's Hospital of Wenzhou Medical University, 325027 Wenzhou, China.

[5]Department of Radiology, Henan Provincial People's Hospital & Zhengzhou University People's Hospital, 450003 Zhengzhou, China.

[6]Biomedical Institute, Henan Academy of Sciences, 450199, Zhengzhou, China.

[7]Department of Radiology, Jinling Hospital, Affiliated Hospital of Medical School, Nanjing University, 210002 Nanjing, China.

[8]Department of Medical Imaging, The Second Hospital of Hebei Medical University, 050000 Shijiazhuang, China.

[9]Department of Radiology, The First Affiliated Hospital of Anhui Medical University, 230022 Hefei, China.

[10]Department of Radiology, Xiangya Hospital, Central South University, 410008 Changsha, China.

[11]Molecular Imaging Research Center of Central South University, 410008 Changsha, China.

[12]National Clinical Research Center for Geriatric Disorders, Xiangya Hospital, Central South University, 410008 Changsha, China.

[13]Department of Radiology, The First Hospital of Shanxi Medical University, 030001 Taiyuan, China.

[14]Department of Radiology, The Affiliated Hospital of Guizhou Medical University, 550004 Guiyang, China.

[15]Department of Radiology, Yantai Yuhuangding Hospital, 264000 Yantai, China.

[16]Department of Radiology, Tianjin Huanhu Hospital, 300350 Tianjin, China.

[17]Department of Radiology, Huashan Hospital, Fudan University, 200040 Shanghai, China.

[18]Department of Radiology, Characteristic Medical Center of Chinese People's Armed Police Force, 300162 Tianjin, China.

[19]School of Medical Imaging and Tianjin Key Laboratory of Functional Imaging, Tianjin Medical University, 300203 Tianjin, China.

[20]Department of Radiology, Tianjin Medical University Cancer Institute & Hospital, National Clinical Research Center for Cancer, Tianjin's Clinical Research Center for Cancer, Tianjin Medical University, Ministry of Education, Key Laboratory of Cancer Prevention and Therapy, Tianjin 300060, China.

[21]Department of Radiology, Huaxi MR Research Center (HMRRC), Functional and Molecular Imaging key Laboratory of Sichuan Province, West China Hospital of Sichuan University, 610041 Chengdu, China.

[22]Research Unit of Psychoradiology, Chinese Academy of Medical Sciences, 610041 Chengdu, China.

[23]Department of Radiology, Hainan General Hospital (Hainan Affiliated Hospital of Hainan Medical University), 570311 Haikou, China.

[24]Department of Magnetic Resonance, Lanzhou University Second Hospital, 730030 Lanzhou, China.

[25]Gansu Province Clinical Research Center for Functional and Molecular Imaging, 730030 Lanzhou, China.

[26]Department of Radiology, Tianjin First Center Hospital, 300192 Tianjin, China.

[27]Department of Radiology, The First Affiliated Hospital of Dalian Medical University, 116011 Dalian, China.

[28]Department of Radiology, Qilu Hospital of Shandong University, 250012 Jinan, China.

[29]Center for MRI Research, Academy for Advanced Interdisciplinary Studies, Peking University, 100871 Beijing, China.

[30]Department of Radiology, The First Affiliated Hospital of Wenzhou Medical University, 325000 Wenzhou, China.

[31]Department of Radiology, Beijing Tongren Hospital, Capital Medical University, 100730 Beijing, China.

[32]Department of Radiology, Tongji Hospital, Tongji Medical College, Huazhong University of Science and Technology, 430030 Wuhan, China.

[33]Department of Radiology, The Affiliated Hospital of Xuzhou Medical University, 221006 Xuzhou, China.

[34]Department of Radiology, Drum Tower Hospital, Medical School of Nanjing University, 210008 Nanjing, China.

[35]Division of Life Science and Medicine, University of Science & Technology of China, 230027 Hefei, China.

[36]Department of Radiology, The First Affiliated Hospital of Guangzhou University of

Chinese Medicine, 510405 Guangzhou, China.

[37]State Key Laboratory of Traditional Chinese Medicine Syndrome, Guangzhou, China.

[38]Functional and Molecular Imaging Key Lab of Shaanxi Province & Department of Radiology, Tangdu Hospital, Air Force Medical University, 710038 Xi'an, China.

[39]Developmental Population Neuroscience Research Center at IDG/McGovern Institute for Brain Research, Beijing Normal University, 100875 Beijing, China.

[40]Institute of Psychology, Chinese Academy of Sciences, 100101 Beijing, China.

[41]These authors contributed equally to this work: Yuan Ji, Caihong Wang, Xiaojun Xu, Zhihan Yan.

[#]Correspondence to:

Chunshui Yu, chunshuiyu@tmu.edu.cn

Xi-Nian Zuo, xinian.zuo@bnu.edu.cn

Guangbin Cui, cuigbtd@163.com

Shijun Qiu, qiu-sj@163.com

Abstract

Perceived thermal stress may offer greater physiological relevance than air temperature; however, its effects on brain-related outcomes remain unclear. We examined persistent effects of lifetime human-perceived thermal stress on lifestyle, brain, and behavior in 5,851 healthy young adults. Longer durations of uncomfortable thermal stress were associated with weaker sour and spicy preferences, higher fish and poultry intake, greater sleep-related daytime dysfunction, smaller cerebral and larger cerebellar volumes, lower white-matter integrity, greater harm avoidance and novelty seeking, lower reward dependence, and reduced psychological well-being. Strong thermal stress was further associated with two additional outcomes. Several cumulative effects showed sensitive periods, with congruent or incongruent effect directions. Although thermal stress affected brain and behavior via direct effects, some behavioral effects were partially mediated by lifestyle alterations. These findings indicate that perceived thermal stress has persistent effects on brain-related outcomes in extraordinarily healthy individuals, supporting its broader use for evaluating thermal-related brain alterations.

Main text

As global temperatures rise, the frequency, duration, and intensity of extreme thermal exposure are continuously increasing[1,2]. The calendar year 2024 marked a milestone: the warmest year on record and the first year in which Earth's surface air temperature exceeded 1.5 °C above preindustrial levels[3]. Extreme thermal exposure has profound influences on health, increasing mortality, morbidity, hospital admissions, and disease burdens across organ systems[4-10]. Regarding brain-related outcomes, extreme thermal exposure, commonly defined using outdoor air temperature, not only affects diseases (e.g., ischemic stroke, Alzheimer's disease, depression, and schizophrenia)[11-14] but also alters brain structure and function[15-17], along with brain-related lifestyle (e.g., sleep and diet)[18,19], personality[20], and behavior (e.g., cognitive and mental health outcomes)[21,22]. However, air temperature does not always match human-perceived thermal stress, as the latter is also influenced by factors such as wind speed, solar radiation, humidity, clothing, and physiological responses[23]. Although human-perceived thermal stress may provide a more biologically relevant measure of thermal exposure[24], its effects on brain structure and function, lifestyle, personality, and behavior remain unclear.

The universal thermal climate index (UTCI) is designed to represent human-perceived thermal stress by translating multidimensional meteorological conditions into an equivalent temperature derived from a validated model of human thermoregulation under standardized assumptions of metabolic activity and clothing insulation[25]. Therefore, UTCI provides a physiologically informed estimate of sustained thermal

burden that extends beyond outdoor air temperature[26]. As global hourly UTCI data are available from 1940 to the present[27], extreme thermal exposure can be assessed using thermal stress duration (TSD): the proportion of hours within a time window during which UTCI exceeded a predefined threshold, such as 26 °C (TSD-26), the upper threshold of thermal comfort, and 32 °C (TSD-32), the lower limit of strong heat stress[23]. Moreover, TSD reflects thermal stress during both daytime and nighttime, capturing nighttime thermal exposure that is commonly neglected by daily maximum temperature assessments—or by those averaged over longer periods.

The Chinese Imaging Genetics (CHIMGEN) study prospectively collected genetic, environmental, behavioral, and neuroimaging data from 7,306 healthy Han Chinese participants aged 18–30 years at 31 research centers across mainland China[28]. Among them, 5,851 participants provided residential coordinates from birth to recruitment, allowing us to derive each participant's time–exposure curve of hourly UTCI values. The comprehensive dataset offers a unique opportunity to address three key questions about the relationship between perceived thermal stress and brain health. First, we can determine whether lifelong human-perceived thermal stress shows persistent effects on brain structure and function, cognitive abilities, personality traits (stable characteristics closely associated with mental health outcomes[29-31]), and mental symptoms in healthy young adults, a very healthy group with a narrow age range that is less likely affected by various confounding factors. Demonstrating significant effects in this group would support using human-perceived thermal stress as a sensitive bioclimate index to assess

the impact of extreme thermal exposure on brain-related outcomes in more vulnerable populations. Second, we can clarify which lifestyle factors mediate the associations between perceived thermal stress and brain-related outcomes, since lifestyle adapts to thermal stress[18,19] and profoundly influences brain and behavior[32,33]. Third, we can identify the age windows during which thermal stress exerts long-lasting effects on adult brain-related outcomes, information critical for targeted interventions.

We addressed these questions in 5,851 healthy young adults from the CHIMGEN cohort with lifetime residential data. We assessed human-perceived thermal stress using lifetime and annual TSD-26 and TSD-32, evaluated brain structure and function with 449 magnetic resonance imaging (MRI) phenotypes, measured lifestyle with 31 items, and examined behavioral outcomes using 11 personality, 10 cognitive, and 7 mental health assessments. First, we investigated the associations of lifetime TSD with lifestyle, neuroimaging, and behavioral outcomes to identify the cumulative effects of lifelong perceived thermal stress on outcomes. Based on identified significant associations, we used distributed lag models (DLMs)[34] to examine the age windows during which annual TSD showed significant associations with adult outcomes, and used structural equation modeling (SEM)[35] to characterize the pathways from lifetime TSD to lifestyle and then to brain and behavioral outcomes. An overview of this study is provided in Fig. 1.

Results

Participants and human-perceived TSD

All participants were Han Chinese recruited through the CHIMGEN study[28]. Inclusion

and exclusion criteria are detailed in Supplementary Table 1. Among the 7,306 healthy participants, 5,851 with complete residential addresses from birth to the date of MRI scanning were included, and hourly UTCI values were extracted from the ERA5-HEAT reanalysis dataset for each participant over this period. Lifetime TSD-26 and TSD-32 were defined as the proportion of lifetime hours with UTCI exceeding 26°C and 32°C, representing uncomfortable and strong thermal stress, respectively. The distributions of these two exposures across the 5,851 participants are shown in Supplementary Fig. 1, with a median of 0.207 (interquartile range, 0.175–0.230) for TSD-26 and 0.084 (interquartile range, 0.066–0.095) for TSD-32.

Overview of association analyses

We investigated associations of each lifetime TSD with 31 lifestyle, 449 brain imaging, and 28 behavioral outcomes. Lifestyle was evaluated by 22 dietary-habit, seven sleep-quality, and two mobile-phone-usage items. Brain structure and function were assessed by grey matter volume (GMV) of 124 regions, surface area (SA) and cortical thickness (CT) of 62 cerebral cortical regions, fractional anisotropy (FA) of 48 white matter tracts, and functional connectivity (BNFC) among 18 resting-state networks (RSNs). Behavior was measured by 11 personality, seven mental health, and ten cognitive assessments. We used multiple imputation by chained equations (MICE)[36] to impute missing data across lifestyle, brain, and behavioral phenotypes, producing ten imputed datasets. The pooled summary statistics across the ten datasets are reported in Supplementary Tables 2-4. In the 5,851 participants, linear regression models were fitted to assess associations

of each lifetime TSD with these imputed phenotypes. All models were adjusted for covariates prespecified by a directed acyclic graph (DAG, Supplementary Figs. 2-3), including age, sex, years of education, family socioeconomic status (SES), and lifetime average normalized difference vegetation index (NDVI). The total intracranial volume (TIV), total SA, mean CT, and mean framewise displacement (FD) were also adjusted in GMV, SA, CT, and BNFC analyses, respectively. We performed regression analyses on each imputed dataset and combined the estimates using Rubin's rules. We adjusted for the effective number (n = 288) of all tests, yielding a significance threshold of $P < 1.74 \times 10^{-4}$ for all association statistics.

Associations between perceived thermal stress and lifestyle outcomes

We examined associations between lifetime TSD and 31 lifestyle outcomes, identifying five associations ($P < 1.74 \times 10^{-4}$) for TSD-26 (Fig. 2a; Supplementary Table 5) and two associations for TSD-32 (Fig. 2b; Supplementary Table 6). Higher TSD-26 was associated with weaker taste preference for sour ($\beta = -0.063$, $P = 1.09 \times 10^{-6}$) and spicy ($\beta = -0.063$, $P = 1.73 \times 10^{-6}$), higher frequency of fish ($\beta = 0.050$, $P = 4.70 \times 10^{-5}$) and poultry ($\beta = 0.043$, $P = 1.36 \times 10^{-4}$) intake, and greater daytime dysfunction of sleep quality ($\beta = 0.054$, $P = 5.80 \times 10^{-5}$). However, higher TSD-32 was only associated with weaker taste preference for sour ($\beta = -0.064$, $P = 3.28 \times 10^{-7}$) and spicy ($\beta = -0.052$, $P = 5.76 \times 10^{-5}$). We performed four sensitivity analyses to assess the robustness of these significant associations. First, we randomly selected 90%, 80%, 70%, and 60% of the 5,851 participants, performing 100 iterations at each proportion (Supplementary Fig.

4). For each proportion, we repeated these seven association analyses for each iteration and aggregated the 100 estimates using variance decomposition, yielding overall effects and their 95% confidence intervals (CIs). The 95% CIs for these seven associations did not include zero and demonstrated the same directions of effect as in the main analysis (Supplementary Fig. 5). We further counted, at each sampling proportion, how many iterations (total n = 100) produced 95% CIs that did not include zero, identifying high counts (86-100; Supplementary Table 7). Second, we replaced linear regression models with proportional-odds logistic regression models to recalculate associations between TSD and 30 ordinal lifestyle outcomes, replicating all associations at $P < 1.74 \times 10^{-4}$ (Supplementary Table 8). The effect sizes for these 30 associations derived from the two models exhibited strong Spearman correlations (TSD-26: *rho* = 0.936, $P = 2.95 \times 10^{-14}$; TSD-32: *rho* = 0.976, $P = 4.52 \times 10^{-20}$; Fig. 2c). Third, to evaluate potential bias from the multiple imputation procedure, we repeated the association analyses using the non-imputed dataset. All seven associations showed similar effect sizes and the same effect directions as in the imputed dataset, and all their 95% CIs did not include zero (Supplementary Fig. 6; Supplementary Tables 9 and 10). Last, to account for the relationship between air temperature and air pollution[37,38], we repeated the association analyses while including fine particulate matter ($PM_{2.5}$), nitrogen dioxide (NO_2), or both as additional covariates. We observed consistent effect directions and 95% CIs excluding zero for all associations (Supplementary Fig. 7; Supplementary Table 11).

For each of the seven significant associations between lifetime TSD and lifestyle

241 outcomes, we used DLMs[34] to identify its sensitive period during the first 18 years of
242 age, defined as the age windows during which the estimated pointwise 95% CI did not
243 include zero. We performed DLMs for each of the 10 imputed datasets and pooled their
244 lag-specific estimates using Rubin's rules. We identified single-year sensitive periods
245 for associations between TSD-26 and four lifestyle outcomes (Supplementary Table 12).
246 Higher TSD-26 at age 8 was associated with stronger sour preference (95% CI, 0.001
247 to 0.080) and with weaker spicy preference (95% CI, -0.086 to -0.001); higher TSD-26
248 at age 5 was associated with less daytime dysfunction of sleep quality (95% CI, -0.106
249 to -0.009); higher TSD-26 at age 17 was associated with higher poultry intake (95% CI,
250 0.00001 to 0.040) (Fig. 2d). For these four associations, the lag-response patterns were
251 consistent across the 10 imputed datasets (Supplementary Fig. 8). However, we did not
252 identify any sensitive age windows for the other three TSD-lifestyle associations.

253 **Associations between perceived thermal stress and brain imaging outcomes**

254 We investigated associations between lifetime TSD and 449 brain imaging outcomes,
255 identifying 14 associations ($P < 1.74 \times 10^{-4}$) for TSD-26 (Supplementary Table 13) and
256 five for TSD-32 (Supplementary Table 14). We found 13 associations between TSD-26
257 and GMV outcomes (Fig. 3a): higher TSD-26 was associated with smaller GMV in 11
258 cerebral regions (Fig. 3b) and with larger GMV in two cerebellar regions (Fig. 3c). Of
259 these, two negative associations with cerebral regions (the left supplementary motor
260 area and inferior occipital gyrus) were also observed for TSD-32 (Fig. 3a). We found
261 that both higher TSD-26 ($\beta = -0.063$, $P = 2.81 \times 10^{-5}$) and TSD-32 ($\beta = -0.058$, $P =$

6.03×10^{-5}) were associated with lower FA in the body of the corpus callosum (Fig. 3d). Across the 14 brain imaging phenotypes, effect estimates for TSD-26 and TSD-32 were directionally concordant and positively correlated (Spearman *rho* = 0.84, $P = 1.60 \times 10^{-4}$). We additionally found that higher TSD-32 was associated with lower FA in the left superior longitudinal fasciculus ($\beta = -0.054$, $P = 1.64 \times 10^{-4}$) and with thinner left lateral occipital cortex ($\beta = -0.054$, $P = 1.15 \times 10^{-6}$). No significant associations were identified between TSD and any other brain imaging outcomes. All 19 associations remained robust across sensitivity analyses, with consistent effect directions and 95% CIs excluding zero under subsampling (Supplementary Fig. 9; Supplementary Table 15), non-imputation (Supplementary Fig. 10; Supplementary Tables 16 and 17), and additional adjustment for air pollutants (Supplementary Fig. 11; Supplementary Table 18).

For each significant TSD-brain association, we used DLMs to identify its sensitive period during the first 18 years of age, identifying sensitive periods for four associations (Supplementary Table 19). Higher TSD-26 at age 1 was associated with larger GMV in the left inferior temporal gyrus (95% CI, 0.001 to 0.075), while higher TSD-26 at ages 12-13 was associated with smaller GMV in the same region (95% CI, -0.074 to -0.003; Fig. 3e); higher TSD-26 at age 3 was linked to smaller GMV in the right supplementary motor area (95% CI, -0.100 to -0.006; Fig. 3f); higher TSD-32 at age 2 was associated with lower FA in the left superior longitudinal fasciculus (95% CI, -0.080 to -0.004; Fig. 3g); higher TSD-32 at ages 0-1 was associated with thinner left lateral occipital

283 cortex (95% CI, -0.121 to -0.002), while higher TSD-32 at ages 8-10 was associated
284 with thicker cortex in the same region (95% CI, 0.002 to 0.070; Fig. 3h). For these four
285 associations, the lag-response patterns were consistent across the 10 imputed datasets
286 (Supplementary Figs. 12 and 13).

287 **Associations between perceived thermal stress and behavioral outcomes**

288 We tested associations between lifetime TSD and 28 behavioral outcomes, identifying
289 four associations ($P < 1.74 \times 10^{-4}$) for TSD-26 (Supplementary Table 20) and two for
290 TSD-32 (Supplementary Table 21). Higher TSD-26 was associated with greater harm
291 avoidance ($\beta = 0.070$, $P = 1.97 \times 10^{-6}$) and novelty seeking ($\beta = 0.067$, $P = 5.34 \times 10^{-6}$),
292 but with lower reward dependence ($\beta = -0.068$, $P = 4.31 \times 10^{-6}$) and well-being ($\beta = -$
293 0.062, $P = 3.72 \times 10^{-5}$) (Fig. 4a); higher harm avoidance ($\beta = 0.056$, $P = 9.46 \times 10^{-5}$)
294 and lower well-being ($\beta = -0.058$, $P = 1.19 \times 10^{-4}$) were also associated with higher
295 TSD-32 (Fig. 4b). All six associations remained robust (consistent effect directions with
296 95% CIs excluding zero) across sensitivity analyses: subsampling (Supplementary Fig.
297 14; Supplementary Table 22), non-imputation (Supplementary Fig. 15; Supplementary
298 Tables 23 and 24) and additional adjustment for air pollutants (Supplementary Fig. 16;
299 Supplementary Table 25).

300 For each significant TSD-behavioral association, we used DLMs to identify its
301 sensitive period during the first 18 years of age, identifying sensitive periods for three
302 associations (Supplementary Table 26). Higher TSD-26 at ages 5-7 was associated with
303 lower novelty seeking (95% CI, -0.138 to -0.006), while higher TSD-26 at age 17 was

304 associated with higher novelty seeking (95% CI, 0.001 to 0.052) (Fig. 4c). Higher TSD-
305 26 at ages 0–1 and 9–11 was associated with lower reward dependence (95% CI, -0.235
306 to -0.003); however, higher TSD-26 at ages 3–6 was associated with higher reward
307 dependence (95% CI, 0.002 to 0.153; Fig. 4d). Higher TSD-32 at age 2 was associated
308 with better well-being (95% CI, 0.003 to 0.081; Fig. 4e). The lag-response patterns of
309 these three associations were consistent across the 10 imputed datasets (Supplementary
310 Figs. 17 and 18).

311 **Thermal stress-lifestyle-brain-behavior pathways**

312 Based on the exposure-outcome associations of TSD-26, we constructed a hierarchical
313 SEM to jointly evaluate the direct and indirect pathways from TSD-26 exposure to brain
314 and behavioral outcomes in the 5,851 participants. In this model, we treated TSD-26 as
315 exposure; lifestyle variables as first-level mediators; brain imaging phenotypes as both
316 second-level mediators and outcomes; and behavioral measures as outcomes only. The
317 pairwise correlation structure across outcomes (Supplementary Fig. 19) guided latent
318 variable construction. Exploratory (EFA) and confirmatory (CFA) factor analyses were
319 used to construct latent variables for 13 highly correlated GMV outcomes. We excluded
320 five outcomes with low loadings (< 0.6) or high cross-loadings ($\geqslant 0.6$) from the initial
321 four-factor solution; the remaining eight GMV outcomes were aggregated into three
322 latent variables: parietal, temporal, and motor GMV. The EFA model explained 74.7%
323 of the total variance and showed a good fit: root mean square residual (RMSR = 0.006),
324 Tucker–Lewis Index (TLI = 0.996), and root mean square error of approximation

(RMSEA = 0.030 [0.022, 0.039]). The factor structure showed high consistency across imputed datasets (Tucker's congruence coefficient = 1.00; Supplementary Fig. 20). The following CFA confirmed the three-factor model (Supplementary Table 27) and showed a good fit: CFI = 0.990, TLI = 0.983, RMSEA = 0.061 [0.056–0.066], and standardized root mean square residual (SRMR = 0.019). Outcomes not included in the three latent variables were treated as independent variables in the SEM, which also showed a good fit (CFI = 0.970, RMSEA = 0.041 [0.040–0.043], and SRMR = 0.026).

Summary statistics for direct and indirect pathways of the final SEM are shown in Fig. 5a, b and Supplementary Tables 28-30. TSD-26 influenced brain outcomes exclusively through direct effects ($|\beta|$ ranging from 0.035 to 0.064, all $P < 0.05$). TSD-26 had negative effects on cerebral regional volumes and white matter FA, but positive effects on cerebellar regional volumes (Fig. 5a; Supplementary Table 28). TSD-26 affected behavioral outcomes primarily through direct effects ($|\beta|$ ranging from 0.038 to 0.070, all $P < 0.05$; Fig. 5a; Supplementary Table 28), although the indirect pathways were also significant ($P < 0.05$; Supplementary Table 30). We found that the association between TSD-26 and harm avoidance was mediated by daytime dysfunction of sleep quality (indirect effect: $\beta = 0.006$, $P = 3.48 \times 10^{-3}$) and fish intake (indirect effect: $\beta = -0.004$, $P = 2.66 \times 10^{-3}$); the association between TSD-26 and novelty seeking was mediated by spicy preference (indirect effect: $\beta = -0.003$, $P = 1.13 \times 10^{-3}$) and poultry intake (indirect effect: $\beta = 0.002$, $P = 3.69 \times 10^{-2}$); the association between TSD-26 and reward dependence was mediated by daytime dysfunction of sleep quality (indirect

effect: β = -0.002, $P = 1.79 \times 10^{-2}$) and fish intake (indirect effect: β = 0.004, $P = 1.96 \times 10^{-3}$); the association between TSD-26 and well-being was mediated by daytime dysfunction of sleep quality (indirect effect: β = -0.017, $P = 2.48 \times 10^{-3}$), fish intake (indirect effect: $\beta = 0.005$, $P = 1.96 \times 10^{-4}$), and the volume of vermis X (indirect effect: β = -0.002, $P = 4.39 \times 10^{-2}$).

Discussion

We conducted a large-scale study investigating long-lasting effects of lifetime human-perceived thermal stress on lifestyle, brain imaging, and behavioral outcomes in 5,851 healthy young adults. We found that longer exposure to uncomfortable thermal stress (TSD-26) was associated with adulthood lifestyle changes, brain structural alterations, personality differences, and poorer mental health. We identified sensitive age windows for several thermal stress effects, with directions either congruent or incongruent with cumulative effects. We revealed that human-perceived thermal stress affected brain and behavior primarily through direct effects, while some behavioral effects were partially mediated by lifestyle alterations. These findings indicate that lifetime perceived thermal stress has persistent effects on lifestyle, brain, and behavior in healthy young adults, and support its use as a sensitive measure for evaluating the effects of extreme thermal exposure on brain-related outcomes in other populations.

This work differs from previous studies in several respects. First, most previous studies used air temperature to assess extreme thermal exposure and then examined its associations with brain-related outcomes[20,39,40], while this study used UTCI, an index

of perceived thermal stress that theoretically confers greater physiological relevance by incorporating additional meteorological variables[25]. Second, we investigated the effects of lifetime thermal stress on brain-related outcomes in healthy adults aged 18-30 years. The stringent inclusion and exclusion criteria (Supplementary Table 1) yielded a very healthy participant group, and the narrow age range minimized interference from both developmental and aging effects. Identifying significant effects of perceived thermal stress on brain-related outcomes in this extraordinarily healthy group would support perceived thermal stress as a sensitive measure for evaluating the impact of extreme thermal exposure on brain-related outcomes across populations, including patients with brain diseases. Third, unlike prior studies that used restricted exposure windows, this study examined the entire lifespan and assessed both cumulative effects and sensitive periods, offering a more complete characterization of strong thermal stress effects on brain-related outcomes. Finally, while previous studies assessed separately the effects of extreme thermal exposure on lifestyle, brain imaging, or behavioral phenotypes, we examined both their individual effects and potential causal relationships, providing information not obtainable from separate analyses.

In the neuroimaging analysis, we found that longer exposure to thermal stress was associated with reduced regional cerebral cortical volumes in healthy adults, consistent with findings for chronic high-temperature exposure in middle-aged and elderly people from the UK Biobank[17]. Unlike previous observations of negative correlations between thermal exposure and regional cerebellar volumes[17], we identified positive correlations.

We also found that both higher TSD-26 and TSD-32 were associated with lower FA in the corpus callosum. As FA is a measure of white matter microstructural integrity, this finding indicates that longer exposure to thermal stress impairs white matter integrity, aligning with the positive correlation between high air temperature and white matter mean diffusivity (MD; higher values indicate worse integrity) in children[15]. However, older individuals exhibited a complex association pattern (coexistence of both positive and negative correlations) between high-temperature exposure and FA and MD[17]. These findings indicate age-specific effects of thermal exposure on brain structural features. Regarding brain function, we did not find any significant associations between thermal stress and between-network functional connectivity, which contrasts with the negative association between 7-day high-temperature exposure and within-network functional connectivity in preadolescents[16]. These results suggest that thermal exposure effects on functional connectivity are transient and do not persist into adulthood, consistent with the observation that the effect was strongest the day before the brain imaging scan and progressively decayed in the preceding days[16]. While effects of TSD-26 and TSD-32 on brain outcomes were highly correlated, TSD-32 was associated with two additional phenotypes: lower FA in the left superior longitudinal fasciculus and thinner left lateral occipital cortex, suggesting that more strong thermal stress leads to additional brain damage.

Unlike prior studies that primarily focused on the effects of acute thermal exposure on diet[41-43], we investigated the long-lasting effects of chronic thermal stress. We found

409 that higher thermal stress was associated with weaker preferences for sour and spicy
410 foods and greater intake of fish and poultry, indicating that chronic thermal exposure
411 alters dietary habits. Consistent with previous reports of degraded sleep quality and
412 quantity caused by high-temperature exposure[44,45], we linked chronic thermal stress to
413 sleep-related daytime dysfunction, manifested as impaired daytime functioning and
414 reduced daytime enthusiasm[46]. Although extreme thermal exposure has been frequently
415 associated with mental health outcomes[22,47], we linked lifetime perceived thermal stress
416 to reduced adulthood psychological well-being in this very healthy group of individuals,
417 consistent with associations between higher temperature and reduced emotional well-
418 being and greater distress in healthy participants[48,49]. Longer thermal stress exposure
419 was associated with personality changes characterized by higher harm avoidance and
420 novelty seeking but lower reward dependence, suggesting greater sensitivity to threat
421 alongside weaker dependence on social reward and attachment[50,51]. These significant
422 effects of lifetime perceived thermal stress on lifestyle and behavior in super-healthy
423 individuals support its use as a sensitive exposure assessment for examining the effects
424 of extreme thermal exposure on more vulnerable populations.

425 When perceived thermal stress had significant cumulative effects on brain-related
426 outcomes, identifying sensitive periods could inform targeted interventions. Sensitive-
427 period analyses revealed complex scenarios with varied preventive implications. Some
428 effects, such as the TSD effect on reduced white matter integrity of the corpus callosum,
429 showed significant cumulative effects but non-significant sensitive periods, suggesting

non-selective preadult interventions. Some effects, such as the TSD effect on reduced volume in the right supplementary motor area, showed both significant cumulative and sensitive-period effects in the same direction, supporting cost-effective interventions during this sensitive period. However, we also observed inconsistencies between the cumulative and sensitive-period effects, such as the effect of TSD-26 on sleep-related daytime dysfunction, indicating that interventions targeting the cumulative effect must avoid the sensitive periods with an opposite effect direction.

Including lifestyle, neuroimaging, and behavioral assessments in the same dataset offers a unique opportunity to characterize the complex effects of thermal stress across these distinct outcome levels. We found that thermal stress influenced brain phenotypes primarily through direct effects, with neuroinflammation as a potential mechanism[52,53]. While thermal stress affected behavioral phenotypes also mainly through direct effects, several associations were mediated by lifestyle factors, such as sleep-related daytime dysfunction, consistent with evidence that poorer sleep quality and daytime dysfunction are associated with emotion regulation difficulties[54], lower psychological well-being[55], and increased vulnerability to mental health problems[56]. These mediations may inform new strategies for reducing the effects of chronic thermal stress on mental health by correcting unhealthy lifestyle factors.

Several limitations should be noted when interpreting our findings. First, thermal stress was estimated based on annual residential locations, which cannot capture within-year mobility or indoor thermal conditions. Second, the cross-sectional neuroimaging

and behavioral data limit causal inference, and diet and sleep assessments relied on self-report rather than objective physiological measures. Third, although statistically robust, the observed effect sizes were modest. Nevertheless, the significant associations found in this exceptionally healthy cohort may indicate stronger impacts of thermal stress on brain-related outcomes in more vulnerable populations. Lastly, this study was restricted to young Han Chinese adults, and therefore generalizability to other populations or age groups requires caution. As brain resilience to environmental stressors varies across the lifespan, different age groups may show distinct sensitivities to thermal stress. Cultural and environmental contexts, including housing conditions and regional lifestyles, may also influence exposure-outcome associations. Future work in diverse populations and climates, ideally with longitudinal neuroimaging and objective physiological measures, will be crucial for clarifying the long-term consequences of sustained thermal stress.

Acknowledgements

We express our gratitude to all CHIMGEN participants and to the researchers who collected and contributed valuable data. This work was supported by the Science & Technology Fundamental Resources Investigation Program (2025FY102300 and 2025FY102302 to C.Y.), National Natural Science Foundation of China (82430063, 82030053 and 81425013 to C.Y.; 82330058 and T2341014 to S.Q.; 82502313 to Y.J.), Tianjin Municipal Health Science and Technology Project (TJWJ2026XK001 to C. Y.), and China National Postdoctoral Program for Innovative Talents (BX 20250242 to Y.J.).

Author Contributions Statement

C.Y. and Y.J. designed the study and wrote the paper. All authors critically reviewed the paper. Y.J., C.W., X.X., Z.Y., M.L., W.Q., F.L., Q.X., J.Xu, N.L., T.J., S.W., H.L., S.Y., S.Q., G.C., X-N.Z. and C.Y. were the principal investigators. C.W., X.X., Z.Y., M.W., L.Z., Z.G., Y. Yu, W. Liao, H.Z., B.G., T.H., Z. Yao, Q.Z., Z. Ye, P.Z., W. Li, W.W., D.S., S.L., F.C., J.Z., W.S., Y.M., D.W., J-H.G., Y. Yang, J. Xian, W.Z., K.X., B.Z., X. Z., S.Q., G.C., X-N.Z. and C.Y. acquired the data. C.Y., X-N.Z., G.C. and S.Q. supervised this work. Y.J. analyzed the data.

Competing Interests Statement

The authors declare no competing interests.

Figure Legends

Fig. 1 | An overview of the study design. a-c, Exposure assessment. Hourly universal

thermal climate index (UTCI) is calculated by integrating air temperature, humidity, solar radiation, and wind speed through physiological and clothing models (**a**). Lifetime hourly UTCI values are extracted for each CHIMGEN participant based on residential coordinates from birth to recruitment (**b**). Lifetime and annual thermal stress durations (TSDs) are then calculated for each participant. For example, lifetime TSD-26 is defined as the proportion of hours during which UTCI exceeds 26°C (**c**). **d-f,** Main analyses. Multivariable linear regression is used to investigate associations between lifetime TSD and adult lifestyle, brain, and behavioral outcomes (**d**). For significant associations, distributed lag models are applied to identify age windows during which annual TSD is associated with outcomes (**e**), and structural equation modeling is then used to characterize direct and indirect pathways from lifetime TSD-26 to lifestyle and subsequently to brain imaging and behavioral outcomes (**f**).

Fig. 2 | Associations between lifetime perceived thermal stress and lifestyle outcomes. a, b, Associations of TSD-26 **(a)** and TSD-32 **(b)** with 31 lifestyle outcomes. The *x*-axis shows standardized β-coefficients and the *y*-axis shows $-\log_{10}(P)$ values. Grey dashed line indicates two-sided $P < 0.05$ and red dashed line indicates two-sided $P < 1.74 \times 10^{-4}$ (Bonferroni corrected). **c,** Concordance between linear regression and proportional-odds logistic regression for associations of TSD-26 (left) and TSD-32 (right) with 30 ordinal lifestyle outcomes. Circles represent associations, with filled circles indicating associations significant at two-sided $P < 1.74 \times 10^{-4}$ in both models. The *x*-axis shows standardized β-estimates from linear regression models and the *y*-axis shows ln(OR)-estimates from logistic regression models. Dashed lines indicate zero effects. **d,** DLMs show sensitive periods during the first 18 years of age for associations between TSD-26 and four lifestyle outcomes. The *x*-axis denotes age at exposure, and the *y*-axis shows standardized β-coefficients. Thick grey vertical lines indicate 95% CIs at each year, whereas thin grey lines represent interpolated values for adjacent years to visualize the continuous temporal pattern. The colored curve demonstrates the smoothed mean effect. Colored vertical bars indicate ages at which the 95% CI for that year does not include zero, corresponding to sensitive age windows.

Fig. 3 | Associations between lifetime perceived thermal stress and brain imaging outcomes. a, Rubin-pooled β-coefficients and 95% CIs for 13 significant associations between TSD-26 and GMV outcomes. **b,** Brain map shows 11 negative associations between TSD-26 and GMV outcomes in the cerebrum. **c,** Brain map shows two positive associations between TSD-26 and GMV outcomes in the cerebellum. **d,** Brain map of the body of the corpus callosum (left) and Rubin-pooled estimates of the associations between TSD-26 and TSD-32 and FA in this region (right). **e-h,** DLMs show sensitive periods during the first 18 years of age for associations between TSD-26 and GMV in the left inferior temporal gyrus (**e**) and right supplementary motor area (**f**) and between TSD-32 and FA in the left superior longitudinal fasciculus (**g**) and CT in the left lateral occipital cortex (**h**). The *x*-axis denotes age at exposure, and the *y*-axis shows standardized β-coefficients. Thick grey vertical lines indicate 95% CI at each year, whereas thin grey lines represent interpolated values for adjacent years to visualize the continuous temporal pattern. The colored curve shows the smoothed mean effect. Colored vertical bars indicate ages at which the 95% CI for that year does not include zero, corresponding to sensitive age windows. Abbreviations: BCC, body of the corpus callosum; CI, confidence interval; L-IOG, left inferior occipital gyrus; L-ITG, left inferior temporal gyrus; L-IX, left cerebellum IX; L-LOC, left lateral occipital cortex; L-PCUN, left precuneus; L-SLF, left superior longitudinal fasciculus; L-SMA, left supplementary motor area; L-TPm, left temporal pole: middle temporal gyrus; R-FFG, right fusiform gyrus; R-ITG, right inferior temporal gyrus; R-PCUN, right precuneus;

536 R-REC, right gyrus rectus; R-SMA, right supplementary motor area; R-SPG, right

537 superior parietal gyrus; VermisX, cerebellar vermis X.

538

Fig. 4 | Associations between lifetime perceived thermal stress and behavioral outcomes. a, b, Associations of TSD-26 **(a)** and TSD-32 **(b)** with 28 behavioral outcomes. The *x*-axis shows standardized β-coefficients and the y-axis shows $-\log_{10}(P)$ values. Grey dashed line indicates two-sided $P < 0.05$ and red dashed line indicates two-sided $P < 1.74 \times 10^{-4}$ (Bonferroni corrected). **c-e,** DLMs show sensitive periods during the first 18 years of age for associations between TSD-26 and novelty seeking (**c**) and reward dependence (**d**) and between TSD-32 and well-being (**e**). The *x*-axis denotes age at exposure, and the *y*-axis shows standardized β-coefficients. Thick grey vertical lines indicate 95% CI at each year, whereas thin grey lines represent interpolated values for adjacent years to visualize the continuous temporal pattern. The colored curve shows the smoothed mean effect. Colored vertical bars indicate ages at which the 95% CI for that year does not include zero, corresponding to sensitive age windows.

Fig. 5 | Direct and indirect pathways from TSD-26 to brain and behavioral outcomes in the final SEM. a, Standardized direct and indirect effects of TSD-26 on brain and behavioral outcomes, estimated in a SEM fitted across 10 imputed datasets and pooled using Rubin's rules. Bars show significant direct and indirect effects ($P < 0.05$, two-sided) of TSD-26 on brain and behavioral outcomes, with lifestyle variables or VermisX as mediators. **b,** The final SEM displays all significant paths among TSD-26, lifestyle measures, brain imaging phenotypes, and behavioral outcomes. Arrow colors indicate the sign of standardized coefficients, and arrow thickness reflects their relative magnitude. Abbreviations: BCC, body of the corpus callosum; DD, daytime dysfunction; DH, dietary habit; FFG, fusiform gyrus; GMV, grey matter volume; HA, harm avoidance; IOG, inferior occipital gyrus; L, left; L-IX, left cerebellum IX; NS, novelty seeking; PSQI, Pittsburgh Sleep Quality Index; R, right; RD, reward dependence; REC, gyrus rectus; SEM, structural equation modeling; TPQ, Tridimensional Personality Questionnaire; TSD, thermal stress duration; VermisX, cerebellar vermis X; WBI, well-being index.

Methods

Ethics approval and participant recruitment

The CHIMGEN protocol was approved by the Medical Ethics Committee of Tianjin Medical University General Hospital (the leading center) and by the ethics committees of the other participating centers (Supplementary Table 31). Written informed consent was obtained from all participants before enrollment. The CHIMGEN study collected genetic, environmental, behavioral, and neuroimaging data from 7,306 healthy Chinese Han participants aged 18–30 years at 31 institutions (32 MRI scanners) across mainland China[28]. Among them, 5,851 participants who provided complete lifetime residential information were included in this analysis. Participants' annual residential addresses were retrospectively collected from birth to the time of MRI acquisition. If a participant moved during a given year, the address where they spent the majority of the year was recorded. Annual residential addresses were converted to latitude and longitude using Google Maps as a basis for subsequent individual-level environmental assessment.

Human-perceived thermal stress assessment

Lifetime hourly UTCI data for all participants were obtained from the ERA5-HEAT dataset (https://cds.climate.copernicus.eu/datasets/derived-utci-historical), produced by the European Centre for Medium-Range Weather Forecasts (ECMWF). This dataset, derived from the ERA5 reanalysis[27], provides global hourly UTCI estimates at a spatial resolution of 0.25° × 0.25° from 1940 to the present. We accessed the data via the climate data store (CDS) and downloaded using the application programming interface

(API) with the *cdsapi* Python package v0.7.5 (https://pypi.org/project/cdsapi/).

For the 5,851 participants, we extracted UTCI data at their residential coordinates from birth date to the date of MRI acquisition. For each calendar year, each participant had only one residential coordinate, based on which we extracted all hourly UTCI values from the nearest grid point to the coordinate using the *xarray* Python package v2025.1.0 (https://pypi.org/project/xarray/). The original UTCI values in Kelvin were converted to degrees Celsius before threshold-based exposure calculations, yielding a continuous lifetime series of hourly thermal stress exposures for each participant. Based on the lifetime series, we computed two cumulative thermal stress exposure indicators: TSD-26 and TSD-32, representing the proportion of lifetime hours during which UTCI exceeded 26 °C and 32 °C, respectively. These thresholds reflect uncomfortable and strong levels of perceived thermal stress. Both indicators were calculated using the following formula:

$$\text{TSD-}x = \frac{N_{\text{UTCI}>x^{\circ}\text{C}}}{N_{\text{total}}}, \text{ where } x = 26 \text{ or } 32$$

where $N_{UTCI>x^{\circ}\text{C}}$ denotes the number of lifetime hours exceeding the threshold (26 °C or 32 °C), and N_{total} is the total number of hours from birth to MRI acquisition.

Lifestyle assessment

We applied 31 items to assess lifestyle from three aspects: dietary habits, sleep quality, and mobile phone usage. Dietary habits were evaluated using 22 items covering the frequency of intake across major food categories (e.g., vegetables, fruits, nuts, meat, dairy, staple grains, and beverages) and individual preferences for saltiness, sweetness,

spiciness, and sourness. Items (Supplementary Methods) were adapted from the UK Biobank diet questionnaire to better reflect Chinese dietary patterns and preferences. Sleep quality was assessed using the Pittsburgh Sleep Quality Index (PSQI)[46], a widely used questionnaire comprising seven items: subjective sleep quality, sleep latency, sleep duration, habitual sleep efficiency, sleep disturbances, use of sleeping medication, and daytime dysfunction. Mobile phone usage was assessed using two items: average daily use was measured on a five-point ordinal scale, and mobile phone dependence was evaluated using the 17-item Mobile Phone Addiction Index (MPAI) scale[57], with higher scores indicating greater dependence. To evaluate collinearity across items, pairwise correlations were computed among the 22 dietary items and among the seven PSQI items (Supplementary Fig. 21).

Brain imaging assessment

Brain imaging data were acquired on thirty-two 3.0-Tesla MRI scanners across 31 sites using standardized scanning parameters (Supplementary Tables 32-34). Details on data quality control, preprocessing, and phenotype extraction procedures are provided in the Supplementary Methods. Structural MRI (sMRI) data were used to calculate regional grey matter volume (GMV), surface area (SA), and cortical thickness (CT). GMV was extracted for 90 cerebral regions defined by the automated anatomical labeling (AAL) atlas[58] and for 34 cerebellar regions defined by the Spatially Unbiased Infra-tentorial (SUIT) template[59]. CT and SA were extracted for 62 cortical regions defined by the Desikan-Killiany-Tourville (DKT) atlas[60]. Diffusion tensor imaging (DTI) data were

used to calculate fractional anisotropy (FA) values for 48 white matter tracts defined by the Johns Hopkins University (JHU) labels[61]. Resting-state functional MRI (rs-fMRI) data were employed to calculate 153 between-network functional connectivity (BNFC) values between 18 non-artefactual resting-state networks (RSNs) identified using group independent component analysis (ICA).

To eliminate scanner effects while retaining biological variability, we performed ComBat harmonization[62] v1.0.1 (https://github.com/Jfortin1/ComBatHarmonization) to harmonize brain imaging phenotypes. The benefit of harmonization was evaluated using repeated scans from two individuals, each of whom had 28 sMRI acquisitions and 26 DTI acquisitions obtained across centers. GMV, CT, SA, and FA were calculated from these scans. For each participant, Spearman correlations were computed between each pair of scanners across all imaging phenotypes within each category (GMV, CT, SA, and FA), yielding between-scanner correlations before and after harmonization. We then used Wilcoxon signed-rank tests to compare within-category correlations before and after harmonization, and found significant improvements (Supplementary Fig. 22; Supplementary Table 35) after harmonization for both participants. Finally, normal score transformation was applied to all harmonized imaging phenotypes to improve normality and mitigate the influence of outliers.

Behavioral assessment

We assessed 28 behavioral variables across three categories: 11 for personality, seven for mental health, and ten for cognitive function.

Personality. Conscientiousness, neuroticism, extraversion, openness to experience, and agreeableness were measured by the NEO Five-Factor Inventory[63]; reward dependence, novelty seeking, and harm avoidance were measured by the Tridimensional Personality Questionnaire (TPQ)[64]; and cognitive impulsiveness (inability to concentrate attention), motor impulsiveness (act without thinking), and non-planning impulsiveness (lack of future planning and forethought) were evaluated by the Barratt Impulsiveness Scale (BIS)[65].

Mental health. Depression was measured by the total score of the 8-item Patient Health Questionnaire (PHQ-8)[66]. State and trait anxiety were evaluated using the State-Trait Anxiety Inventory (STAI)[67]. Subjective psychological well-being was measured by the total score of the WHO Five Well-Being Index (WHO-5)[68]. Perceived stress was measured by the total score of the 10-item Perceived Stress Scale (PSS-10)[69]. Emotional state was assessed using the Positive and Negative Affect Schedule (PANAS)[70], yielding positive (PANAS-PA) and negative (PANAS-NA) affect scores.

Cognitive function. Five standardized tasks were used to assess cognitive function. Working memory was assessed using a letter N-back task[71]. In the 1-back and 3-back blocks, participants judged whether the current letter matched the one presented one and three trials earlier, respectively. Each block comprised 60 stimuli presented for 200 ms at 1,800-ms intervals via E-Prime v2.0. Only participants whose correct rate (CR) exceeded 75% in the 1-back practice proceeded to the formal test. Working memory was evaluated using the correct rate in the 3-back task (N-back CR). Verbal learning

674 and memory were assessed using the second edition of the California Verbal Learning
675 Test (CVLT-II)[72]. Participants were presented with two word lists (A and B), each
676 consisting of 16 words. List A was learned and recalled across five immediate trials,
677 followed by a single trial of the interference List B. Subsequent recall phases included
678 a short delay (immediately after the interference trial) and a long delay (20 minutes
679 later), during which participants completed both free and cued recall of List A. Five
680 outcome measures were derived from the number of correctly recalled words:
681 immediate free recall, short delayed free recall, short delayed cued recall, long delayed
682 free recall, and long delayed cued recall. Visuospatial memory was assessed using the
683 Rey–Osterrieth Complex Figure Test (ROCFT)[73]. Participants were asked to copy a
684 complex line figure, then redraw it from memory immediately and again after a 25-
685 minute delay. A 36-point scoring system was used to evaluate performance in each
686 phase, based on standardized scoring criteria. The immediate and delayed recall scores
687 were used to quantify visuospatial memory. To minimize inter-rater variability, all
688 assessments were rated by a trained and fixed group of raters. Executive control was
689 evaluated using a Go/No-Go task[74]. Participants viewed a continuous stream of letters
690 and were instructed to press a button whenever the current letter differed from the one
691 immediately preceding it (“go” trials, 90%) and to withhold their response when the
692 same letter appeared twice in a row (“no-go” trials, 10%). The task was programmed
693 and administered using E-Prime v2.0. The correct response rate in no-go trials (No-Go
694 CR) was used as an index of executive control. Social fairness decision-making was

assessed using an Ultimatum Game presented by E-Prime v2.0[75]. Each participant acted as a responder, deciding whether to accept or reject monetary offers (e.g., 2:8 split) proposed by another player for dividing a fixed sum of ten yuan. Acceptance led to both players receiving the proposed amounts; rejection resulted in neither player receiving any money. The acceptance rate of the 2:8 allocation scheme in the Ultimatum Game (UG-AR) was used to quantify fairness-related decision-making.

Behavioral data quality control. All behavioral variables were screened for out-of-range values based on their respective valid response ranges (e.g., scale boundaries or logical constraints). Values falling outside the expected range were treated as missing and subsequently imputed. Normal score transformation was also applied to behavioral phenotypes to improve normality and mitigate the impact of outliers prior to statistical analyses.

Covariates

A directed acyclic graph (DAG) was constructed to illustrate the hypothesized causal relationships among TSD, brain image phenotypes or behavioral traits, and potential confounders[76] (Supplementary Figs. 2 and 3). Based on this framework, the *dagitty* R package v0.3.4 (https://cran.r-project.org/web/packages/dagitty/index.html) was used to identify minimal sufficient adjustment sets for confounding control. Three candidate adjustment sets were generated: (1) individual education level, family socioeconomic status (SES), and normalized difference vegetation index (NDVI); (2) family SES, individual education level, and residential address; (3) NDVI, residential address, and

urbanicity. Given the difficulty of integrating multiple residential addresses across the lifespan into a single reliable measure, we abandoned the latter two sets and selected the first set (family SES, individual education level, and NDVI) as covariates.

We employed each participant's lifetime-averaged NDVI value as the covariate, calculated from the annual NDVI values at the participant's residential coordinates. Annual values were extracted from the Landsat Collection 2 Tier 1 Level 2 Annual NDVI Composite in Google Earth Engine (https://developers.google.com/earth-engine/datasets/catalog/LANDSAT_COMPOSITES_C02_T1_L2_ANNUAL_NDVI?hl=zh-cn#bands), which provides annual NDVI composites at 30 m spatial resolution from 1984 onward. Family SES was defined using the first latent factor from a validated SES factor structure[77], which was derived via factor analyses of 16 SES indicators. The first factor reflected family-level SES, characterized by parental education, parental occupation, household income, and family wealth and resources. Individual education level was assessed as total years of formal education. We also included age, sex, and several outcome-specific covariates, comprising total intracranial volume (TIV) for GMV outcomes; hemisphere-specific mean CT for CT outcomes; hemisphere-specific total SA for SA outcomes; and mean Jenkinson FD[78] for BNFC outcomes.

Multiple imputation by chained equations (MICE)

To address missing data, we performed multiple imputation using MICE with the *mice* R package v3.18.0 (https://cran.r-project.org/web/packages/mice/index.html). A total of 508 outcomes, including 449 brain imaging phenotypes, 31 lifestyle variables, and

28 behavioral outcomes, together with all relevant exposure variables and covariates, were jointly included in the imputation model. All missing rates were below 40% (Supplementary Table 36, Supplementary Fig. 23), a range in which MICE has been shown to perform robustly across missingness scenarios, including the departure from the missing at random (MAR) assumption[79]. We performed imputation using a sample-splitting strategy analogous to 10-fold cross-fitting: the dataset was split into ten folds, and in each fold, missing values were imputed only for participants in that fold using imputation models estimated from the remaining nine folds. Ten complete datasets were generated using predictive mean matching with the default settings and 20 iterations.

Statistical analysis

Linear regression was used to examine associations of TSD-26 and TSD-32 with 449 brain imaging, 31 lifestyle, and 28 behavioral outcomes. The *FRGEpistasis* R package v1.42.0 (https://bioconductor.org/packages/release/bioc/html/FRGEpistasis.html) was used to perform a rank-based inverse normal transform to make all continuous variables approximate Gaussian distributions prior to model fitting. Covariates included age, sex, individual-level education, family SES, and NDVI in all analyses, along with outcome-specific covariates for particular analyses. We conducted analyses on the ten imputed datasets separately, and used Rubin's rules to pool the regression estimates. To balance the multiple-testing burden and the correlated structure among outcomes, we calculated the effective number of independent tests (M_{eff}) from the eigenvalues of the correlation matrix using the proposed approach[80], implemented in the *poolr* R package v1.2.0

(https://cran.r-project.org/web/packages/poolr/index.html). M_{eff} value was calculated for each imputed dataset based on the correlation matrix of 508 outcomes. The resulting M_{eff} values ranged from 287 to 289 across datasets, and the mean M_{eff} = 288 was used to determine the adjusted significance threshold. All statistics were performed in R v4.3.1 (https://www.r-project.org/) and Python v3.11.4 (https://www.python.org/).

Sensitivity analysis

First, to evaluate the robustness of significant associations identified in the full sample (n = 5,851), we randomly drew 90%, 80%, 70%, and 60% of the full sample without replacement, repeating 100 iterations at each proportion (Supplementary Fig. 4). For each iteration, the same analytic pipeline was applied to estimate the exposure–outcome associations in each of the 10 imputed datasets, and the results were pooled using Rubin's rules to yield one iteration-level effect estimate. For each sampling proportion, the 100 iteration-level effect estimates were combined using a within–between variance decomposition, in which the average within-iteration and between-iteration variances were jointly used to estimate the overall effect and its 95% confidence interval (CI). Associations were considered robust when the aggregated 95% CI did not include zero. We additionally calculated the proportion of iterations whose 95% CI did not include zero for each subsampling proportion.

Second, given that among the 508 outcome variables only 30 were ordinal (5.9%), the main analyses were uniformly implemented using linear regression. To account for their ordinal nature, we fitted proportional-odds ordinal logistic regression using the

MASS R package v7.3.65 (https://cran.r-project.org/web/packages/MASS/index.html) for the 30 ordinal outcomes within each imputed dataset, and pooled the estimates using Rubin's rules. Pooled odds ratios (ORs) with 95% CIs were reported.

Third, to evaluate the robustness of the results to the imputation procedure, we repeated all regression analyses in participants with complete data. Linear regression models and covariates were identical to those used in the main analyses. Spearman's rank correlation was calculated between the standardized β estimates obtained from the imputed and non-imputed datasets across the associations that were significant in the imputed analyses ($P < 1.74 \times 10^{-4}$).

Fourth, considering the complex and not yet fully understood relationship between temperature and air pollution[37,38], air pollutants were included as additional covariates in sensitivity analyses. Fine particulate matter ($PM_{2.5}$) was treated as the predominant pollutant because of consistent evidence of its impact on brain structure and cognitive function[81-84], while nitrogen dioxide (NO_2) was included based on emerging evidence of its potential effects[85,86]. $PM_{2.5}$ exposure was derived from the Global Annual $PM_{2.5}$ Grids V5.GL.04 (MODIS, MISR, SeaWiFS AOD), which provide annual $PM_{2.5}$ concentrations (ug/m^3) at a spatial resolution of 0.1° × 0.1° for the period 1998–2022 (https://www.earthdata.nasa.gov/data/catalog/sedac-ciesin-sedac-sdei-gwrpm25-mmsvaod-5gl04-5.04). Annual ground-level NO_2 concentrations (parts per billion, ppb) were obtained from SEDAC (https://sedac.ciesin.columbia.edu/data/set/sdei-global-3-year-running-mean-no2-gome-sciamachy-gome2), provided as global 3-year running

mean grids at a spatial resolution of 0.1° (about 11 km) and covering the period from 1997 to 2011. For each participant, annual $PM_{2.5}$ and NO_2 concentrations were averaged across all available years to derive long-term exposure estimates. Sensitivity analyses re-estimated all models adjusted for $PM_{2.5}$ alone, NO_2 alone, or both simultaneously. All models were fitted across the 10 imputed datasets and combined using Rubin's rules. Robustness was assessed by examining whether associations from the main analyses remained significant in this sensitivity analysis.

Distributed lag modeling

We used a distributed lag model (DLM) framework with the *dlnm* R package v2.4.10 (https://cran.r-project.org/web/packages/dlnm/index.html) to characterize the temporal distribution of TSD exposure effects from birth to late adolescence (0–18 years) and to identify age-specific susceptibility windows. Yearly exposures to TSD-26 and TSD-32 were aligned with each participant's birth year to construct lag spaces covering the developmental period (0–18 years). Before model fitting, exposures were standardized to ensure comparability across participants and years. A cross-basis was specified with a linear exposure–response function and a smooth lag–response function modeled using a natural cubic spline with 7 degrees of freedom. Each model included the same set of covariates as those used in the main analyses. DLMs were fitted in ten imputed datasets, and lag-specific estimates and CIs were combined using Rubin's rules. Developmental windows were defined as contiguous lags where the pooled 95% CIs did not include zero.

Structural equation modeling (SEM)

Based on all significant associations between TSD-26 and outcomes, we constructed a hierarchical SEM to evaluate the direct and indirect pathways from TSD-26 to brain and behavioral outcomes in the 5,851 participants. The SEM treated TSD as exposure; lifestyle variables as first-level mediators; brain imaging phenotypes as both second-level mediators and outcomes; and behavioral measures as outcomes only. We assessed Pearson correlations among outcomes associated with TSD-26, averaged across the ten imputed datasets (Supplementary Fig. 19). We constructed latent variables for highly correlated outcomes using exploratory (EFA) and confirmatory (CFA) factor analyses with the *psych* R v2.5.6 (https://cran.r-project.org/web/packages/psych/index.html) and the *lavaan.mi* R v0.1.0 (https://cran.r-project.org/web/packages/lavaan.mi/index.html). A parallel analysis (1,000 iterations) was applied to the imputed datasets to determine the number of latent variables. After excluding outcomes with low loadings (< 0.6) or high cross-loadings ($\geqslant 0.6$), the remaining outcomes were entered into a second round of parallel analysis. EFA fit was evaluated using the root mean square residual (RMSR), Tucker–Lewis Index (TLI), and root mean square error of approximation (RMSEA). Tucker's congruence coefficient was used to assess the consistency of factor structures across imputations. CFA was performed to define the SEM latent constructs across imputed datasets; model fit was evaluated using the comparative fit index (CFI), TLI, RMSEA, and standardized root mean square residual (SRMR). Outcomes not included in latent variables were treated as independent variables in the SEM model. The final

SEM was estimated using the *lavaan.mi* R package, which combined results across imputed datasets and adjusted for covariates consistent with association analyses. Model fit was assessed using CFI, RMSEA, and SRMR.

Data Availability

ERA5-HEAT UTCI data accessed via the Climate Data Store (https://cds.climate.copernicus.eu/datasets/derived-utci-historical). NDVI was derived in Google Earth Engine using the Landsat Collection 2 Tier 1 Level 2 Annual NDVI Composite (https://developers.google.com/earth-engine/datasets/catalog/LANDSAT_COMPOSITES_C02_T1_L2_ANNUAL_NDVI?hl=zh-cn#bands). Sensitivity analyses used $PM_{2.5}$ from the Global Annual $PM_{2.5}$ Grids V5.GL.04 (https://www.earthdata.nasa.gov/data/catalog/sedac-ciesin-sedac-sdei-gwrpm25-mmsvaod-5gl04-5.04) and NO_2 from the Global 3-year Running Mean NO_2 grids (https://sedac.ciesin.columbia.edu/data/set/sdei-global-3-year-running-mean-no2-gome-sciamachy-gome2).

Code Availability

ERA5-HEAT UTCI data were extracted with cdsapi (v0.7.5, https://pypi.org/project/cdsapi/) and xarray (v2025.1.0, https://pypi.org/project/xarray/). Harmonization was conducted using ComBat harmonization (v1.0.1 https://github.com/Jfortin1/ComBatHarmonization). All statistical analyses in this study were conducted using R v4.3.1 (https://www.r-project.org/) and Python v3.11.4 (https://www.python.org/), with key R packages including mice v3.18.0 (https://cran.r-project.org/web/packages/mice/index.html), dlnm v2.4.10 (https://cran.r-project.org/web/packages/dlnm/index.html), psych v2.5.6 (https://cran.r-

project.org/web/packages/psych/index.html), lavaan.mi v0.1.0 (https://cran.r-project.org/web/packages/lavaan.mi/index.html), poolr (https://cran.r-project.org/web/packages/poolr/index.html), dagitty (https://cran.r-project.org/web/packages/dagitty/index.html), MASS (https://cran.r-project.org/web/packages/MASS/index.html), and FRGEpistasis v1.42.0 (https://bioconductor.org/packages/release/bioc/html/FRGEpistasis.html).

References

1. Murali, G., Iwamura, T., Meiri, S. & Roll, U. Future temperature extremes threaten land vertebrates. *Nature* **615**, 461-467 (2023).
2. Martinez-Villalobos, C., Fu, D., Loikith, P.C. & Neelin, J.D. Accelerating increase in the duration of heatwaves under global warming. *Nat Geosci* **18**, 716-723 (2025).
3. Bevacqua, E., Schleussner, C.-F. & Zscheischler, J. A year above 1.5 °C signals that Earth is most probably within the 20-year period that will reach the Paris Agreement limit. *Nature Climate Change* **15**, 262-265 (2025).
4. Wu, X.*, et al.* Future heat-related mortality in Europe driven by compound day-night heatwaves and demographic shifts. *Nat Commun* **16**, 7420 (2025).
5. Xi, D.*, et al.* Risk factors associated with heatwave mortality in Chinese adults over 65 years. *Nat Med* **30**, 1489-1498 (2024).
6. Liu, J.*, et al.* Rising cause-specific mortality risk and burden of compound heatwaves amid climate change. *Nature Climate Change* **14**, 1201-1209 (2024).
7. Cheng, J.*, et al.* Cardiorespiratory effects of heatwaves: A systematic review and meta-analysis of global epidemiological evidence. *Environ Res* **177**, 108610 (2019).
8. Crandall, C.G. & Gonzalez-Alonso, J. Cardiovascular function in the heat-stressed human. *Acta Physiol (Oxf)* **199**, 407-423 (2010).
9. Zhang, Y., Yu, C. & Wang, L. Temperature exposure during pregnancy and birth outcomes: An updated systematic review of epidemiological evidence. *Environ Pollut* **225**, 700-712 (2017).
10. Sisodiya, S.M.*, et al.* Climate change and disorders of the nervous system. *Lancet Neurol* **23**, 636-648 (2024).
11. Culqui, D.R., Linares, C., Ortiz, C., Carmona, R. & Diaz, J. Association between environmental factors and emergency hospital admissions due to Alzheimer's disease in Madrid. *Sci Total Environ* **592**, 451-457 (2017).
12. Gong, J., Part, C. & Hajat, S. Current and future burdens of heat-related dementia hospital admissions in England. *Environ Int* **159**, 107027 (2022).
13. Zhang, R.*, et al.* Effect of heatwaves on mortality of Alzheimer's disease and other dementias among elderly aged 60 years and above in China, 2013-2020: a population-based study. *Lancet Reg Health West Pac* **52**, 101217 (2024).
14. Delaney, S.W.*, et al.* Extreme Heat and Hospitalization Among Older Persons With Alzheimer Disease and Related Dementias. *JAMA Intern Med* **185**, 412-421 (2025).
15. Granés, L.*, et al.* Early life cold and heat exposure impacts white matter development in children. *Nature Climate Change* **14**, 760-766 (2024).
16. Granes, L.*, et al.* Exposure to Ambient Temperature and Functional Connectivity of Brain Resting-State Networks in Preadolescents. *J Am Acad Child Adolesc Psychiatry* **64**, 1317-1328 (2025).
17. Xiang, W.*, et al.* Chronic high temperature exposure, brain structure, and mental health: Cross-sectional and prospective studies. *Environ Res* **264**, 120348 (2025).
18. He, P., Xu, Z., Chan, D., Liu, P. & Bai, Y. Rising temperatures increase added sugar

intake disproportionately in disadvantaged groups in the USA. *Nature Climate Change* **15**, 963-970 (2025).
19. Li, A.*, et al.* Climate warming may undermine sleep duration and quality in repeated-measure study of 23 million records. *Nat Commun* **16**, 2609 (2025).
20. Wei, W.*, et al.* Regional ambient temperature is associated with human personality. *Nat Hum Behav* **1**, 890-895 (2017).
21. Yin, B.*, et al.* Effect of extreme high temperature on cognitive function at different time scales: A national difference-in-differences analysis. *Ecotoxicol Environ Saf* **275**, 116238 (2024).
22. Thompson, R.*, et al.* Ambient temperature and mental health: a systematic review and meta-analysis. *Lancet Planet Health* **7**, e580-e589 (2023).
23. Brode, P.*, et al.* Deriving the operational procedure for the Universal Thermal Climate Index (UTCI). *Int J Biometeorol* **56**, 481-494 (2012).
24. Emerton, R., Nicolas, J., Lombardi, A. & Di Napoli, C. Global heat stress intensification and its expanding footprint on the human population. *Nature Climate Change* (2026).
25. Fiala, D., Havenith, G., Brode, P., Kampmann, B. & Jendritzky, G. UTCI-Fiala multi-node model of human heat transfer and temperature regulation. *Int J Biometeorol* **56**, 429-441 (2012).
26. Romaszko, J., Draganska, E., Jalali, R., Cymes, I. & Glinska-Lewczuk, K. Universal Climate Thermal Index as a prognostic tool in medical science in the context of climate change: A systematic review. *Sci Total Environ* **828**, 154492 (2022).
27. Di Napoli, C., Barnard, C., Prudhomme, C., Cloke, H.L. & Pappenberger, F. ERA5-HEAT: A global gridded historical dataset of human thermal comfort indices from climate reanalysis. *Geoscience Data Journal* **8**, 2-10 (2020).
28. Xu, Q.*, et al.* CHIMGEN: a Chinese imaging genetics cohort to enhance cross-ethnic and cross-geographic brain research. *Molecular psychiatry* **25**, 517-529 (2020).
29. Kotov, R., Gamez, W., Schmidt, F. & Watson, D. Linking "big" personality traits to anxiety, depressive, and substance use disorders: a meta-analysis. *Psychol Bull* **136**, 768-821 (2010).
30. Gurpegui, D., Ortuno, F. & Gurpegui, M. Temperament traits and remission of depression: A naturalistic six-month longitudinal study. *J Affect Disord* **243**, 494-502 (2019).
31. Zhong, S.*, et al.* Neural correlates of harm avoidance: a multimodal meta-analysis of brain structural and resting-state functional neuroimaging studies. *Transl Psychiatry* **14**, 384 (2024).
32. Chen, H.*, et al.* Associations of the Mediterranean-DASH Intervention for Neurodegenerative Delay diet with brain structural markers and their changes. *Alzheimers Dement* **20**, 1190-1200 (2024).
33. Li, Y.*, et al.* The brain structure and genetic mechanisms underlying the nonlinear association between sleep duration, cognition and mental health. *Nat Aging* **2**, 425-437 (2022).

34. Gasparrini, A., Armstrong, B. & Kenward, M.G. Distributed lag non-linear models. *Stat Med* **29**, 2224-2234 (2010).
35. Bollen, K.A. The General Model, Part I: Latent Variable and Measurement Models Combined. in *Structural Equations with Latent Variables* 319-394 (Wiley, 1989).
36. White, I.R., Royston, P. & Wood, A.M. Multiple imputation using chained equations: Issues and guidance for practice. *Stat Med* **30**, 377-399 (2011).
37. Buckley, J.P., Samet, J.M. & Richardson, D.B. Commentary: Does air pollution confound studies of temperature? *Epidemiology* **25**, 242-245 (2014).
38. Kalisa, E., Fadlallah, S., Amani, M., Nahayo, L. & Habiyaremye, G. Temperature and air pollution relationship during heatwaves in Birmingham, UK. *Sustainable Cities and Society* **43**, 111-120 (2018).
39. Cedeno Laurent, J.G.*, et al.* Reduced cognitive function during a heat wave among residents of non-air-conditioned buildings: An observational study of young adults in the summer of 2016. *PLoS Med* **15**, e1002605 (2018).
40. Hsiang, S.M., Burke, M. & Miguel, E. Quantifying the influence of climate on human conflict. *Science* **341**, 1235367 (2013).
41. Millet, J.*, et al.* Effects of Acute Heat and Cold Exposures at Rest or during Exercise on Subsequent Energy Intake: A Systematic Review and Meta-Analysis. *Nutrients* **13**(2021).
42. Coca, M.*, et al.* Twenty four-hour passive heat and cold exposures did not modify energy intake and appetite but strongly modify food reward. *Br J Nutr* **132**, 209-226 (2024).
43. Motoki, K., Saito, T., Nouchi, R., Kawashima, R. & Sugiura, M. The paradox of warmth: Ambient warm temperature decreases preference for savory foods. *Food Quality and Preference* **69**, 1-9 (2018).
44. Chevance, G.*, et al.* A systematic review of ambient heat and sleep in a warming climate. *Sleep Med Rev* **75**, 101915 (2024).
45. Griggs, S., Harper, A. & Hickman, R.L., Jr. A systematic review of sleep deprivation and neurobehavioral function in young adults. *Appl Nurs Res* **63**, 151552 (2022).
46. Buysse, D.J., Reynolds, C.F., 3rd, Monk, T.H., Berman, S.R. & Kupfer, D.J. The Pittsburgh Sleep Quality Index: a new instrument for psychiatric practice and research. *Psychiatry Res* **28**, 193-213 (1989).
47. Nori-Sarma, A.*, et al.* Association Between Ambient Heat and Risk of Emergency Department Visits for Mental Health Among US Adults, 2010 to 2019. *JAMA Psychiatry* **79**, 341-349 (2022).
48. Noelke, C.*, et al.* Increasing ambient temperature reduces emotional well-being. *Environ Res* **151**, 124-129 (2016).
49. Tawatsupa, B.*, et al.* Heat stress, health and well-being: findings from a large national cohort of Thai adults. *BMJ Open* **2**(2012).
50. Cloninger, C.R., Svrakic, D.M. & Przybeck, T.R. A psychobiological model of temperament and character. *Arch Gen Psychiatry* **50**, 975-990 (1993).
51. De Fruyt, F., Van De Wiele, L. & Van Heeringen, C. Cloninger's Psychobiological

Model of Temperament and Character and the Five-Factor Model of Personality. *Personality and Individual Differences* **29**, 441-452 (2000).

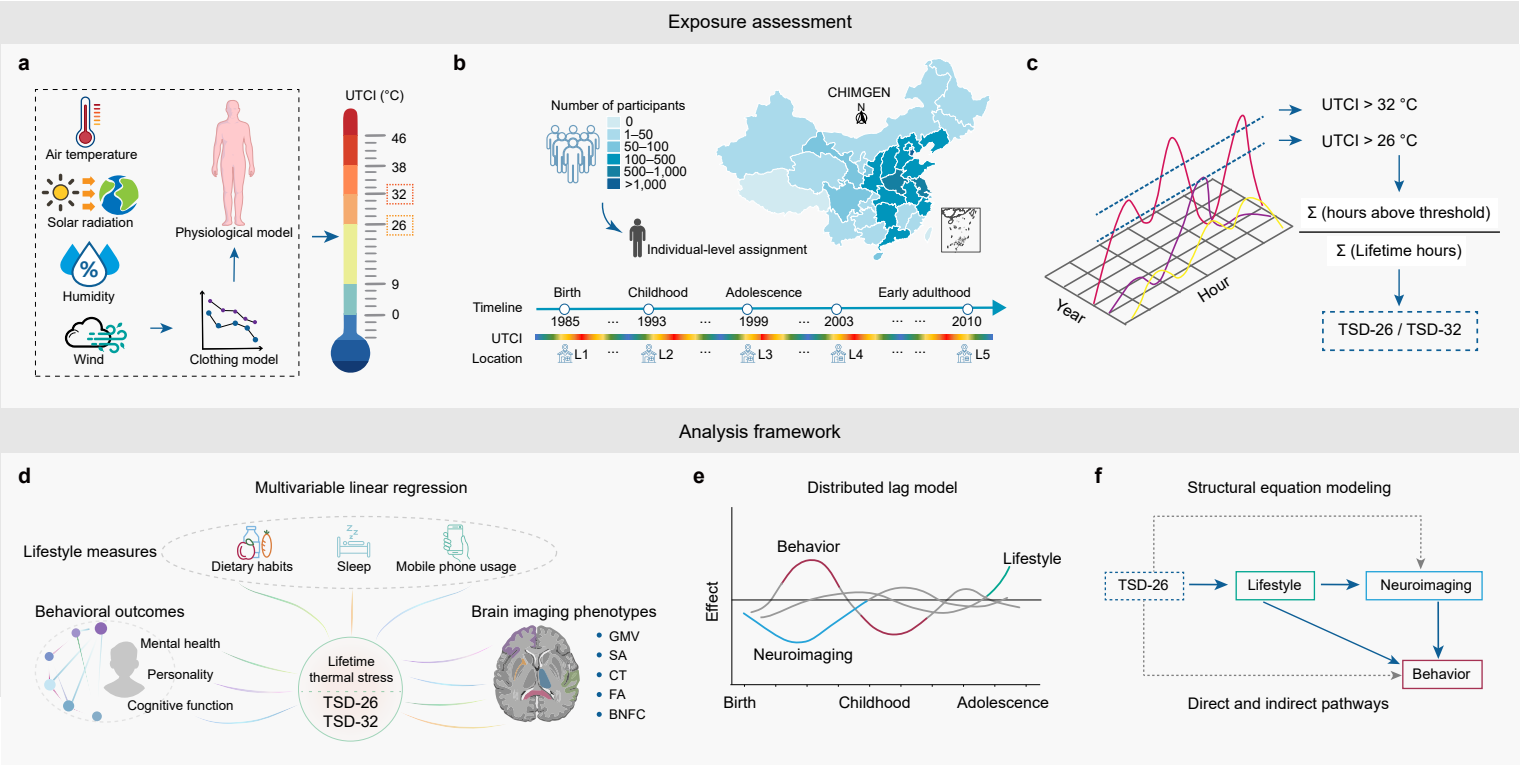
52. Lee, W., Moon, M., Kim, H.G., Lee, T.H. & Oh, M.S. Heat stress-induced memory impairment is associated with neuroinflammation in mice. *J Neuroinflammation* **12**, 102 (2015).
53. Bouchama, A.*, et al.* Classic and exertional heatstroke. *Nat Rev Dis Primers* **8**, 8 (2022).
54. Wang, W.*, et al.* The impact of sleep quality on emotion regulation difficulties in adolescents: a chained mediation model involving daytime dysfunction, social exclusion, and self-control. *BMC Public Health* **24**, 1862 (2024).
55. Espie, C.A.*, et al.* Effect of Digital Cognitive Behavioral Therapy for Insomnia on Health, Psychological Well-being, and Sleep-Related Quality of Life: A Randomized Clinical Trial. *JAMA Psychiatry* **76**, 21-30 (2019).
56. Freeman, D.*, et al.* The effects of improving sleep on mental health (OASIS): a randomised controlled trial with mediation analysis. *Lancet Psychiatry* **4**, 749-758 (2017).
57. Leung, L. Linking Psychological Attributes to Addiction and Improper Use of the Mobile Phone among Adolescents in Hong Kong. *Journal of Children and Media* **2**, 93-113 (2008).
58. Tzourio-Mazoyer, N.*, et al.* Automated anatomical labeling of activations in SPM using a macroscopic anatomical parcellation of the MNI MRI single-subject brain. *NeuroImage* **15**, 273-289 (2002).
59. Diedrichsen, J., Balsters, J.H., Flavell, J., Cussans, E. & Ramnani, N. A probabilistic MR atlas of the human cerebellum. *NeuroImage* **46**, 39-46 (2009).
60. Desikan, R.S.*, et al.* An automated labeling system for subdividing the human cerebral cortex on MRI scans into gyral based regions of interest. *NeuroImage* **31**, 968-980 (2006).
61. Wakana, S.*, et al.* Reproducibility of quantitative tractography methods applied to cerebral white matter. *NeuroImage* **36**, 630-644 (2007).
62. Fortin, J.P.*, et al.* Harmonization of multi-site diffusion tensor imaging data. *NeuroImage* **161**, 149-170 (2017).
63. Costa, P. & McCrae, R. NEO five-factor inventory (NEO-FFI). *Odessa, FL: Psychological Assessment Resources* **3**(1989).
64. Cloninger, C.R., Przybeck, T.R. & Svrakic, D.M. The tridimensional personality questionnaire: US normative data. *Psychological reports* **69**, 1047-1057 (1991).
65. Patton, J.H., Stanford, M.S. & Barratt, E.S. Factor structure of the Barratt impulsiveness scale. *Journal of clinical psychology* **51**, 768-774 (1995).
66. Kroenke, K.*, et al.* The PHQ-8 as a measure of current depression in the general population. *J Affect Disord* **114**, 163-173 (2009).
67. Spielberger, C.D. *Manual for the State-Trait Anxiety Inventory STAI (form Y)(" self-evaluation questionnaire")*, (Consulting Psychologists Press, Palo Alto, CA, 1983).
68. Topp, C.W., Ostergaard, S.D., Sondergaard, S. & Bech, P. The WHO-5 Well-Being

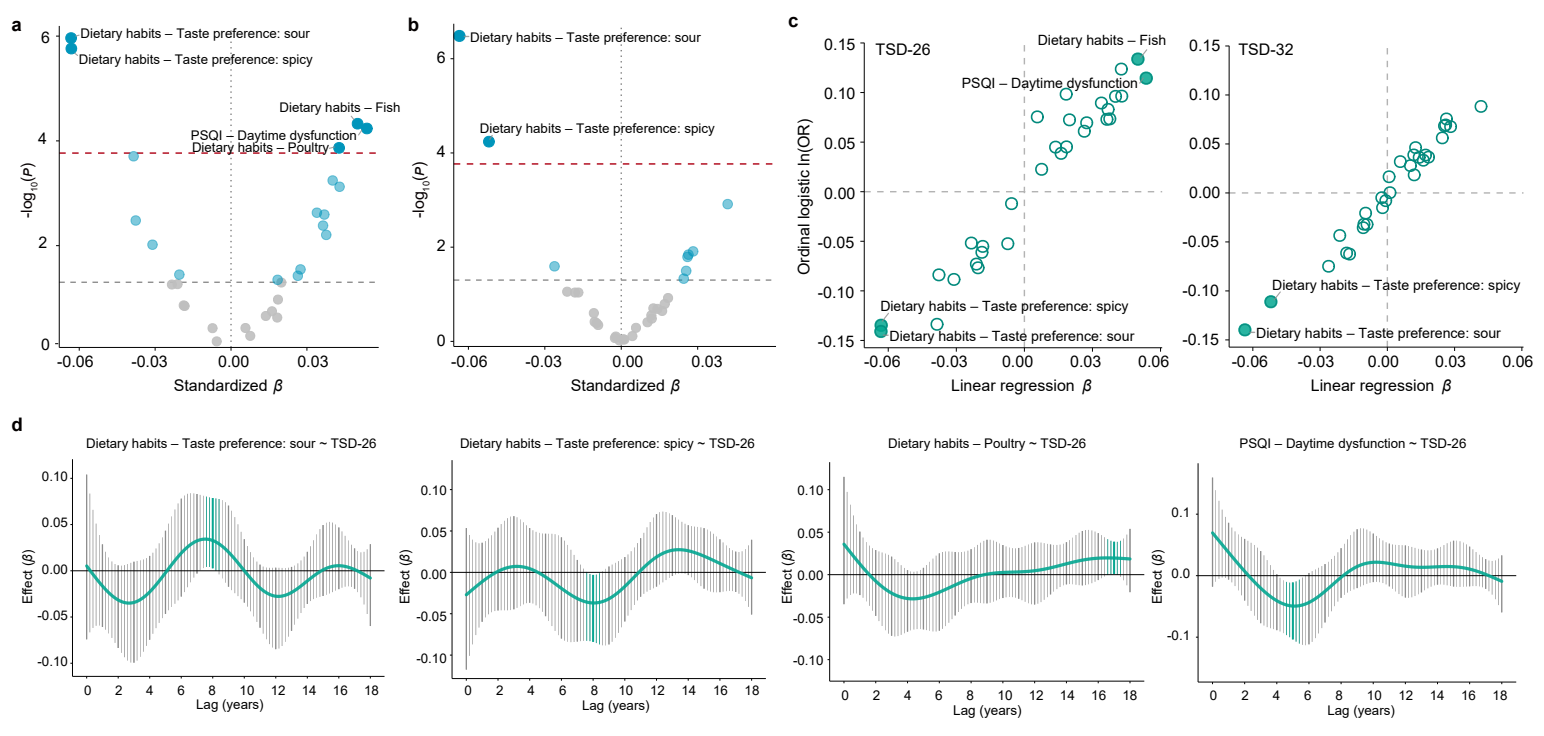
Index: a systematic review of the literature. *Psychother Psychosom* **84**, 167-176 (2015).
69. Cohen, S., Kamarck, T. & Mermelstein, R. A global measure of perceived stress. *J Health Soc Behav* **24**, 385-396 (1983).
70. Watson, D., Clark, L.A. & Tellegen, A. Development and validation of brief measures of positive and negative affect: the PANAS scales. *Journal of personality and social psychology* **54**, 1063-1070 (1988).
71. Owen, A.M., McMillan, K.M., Laird, A.R. & Bullmore, E. N-back working memory paradigm: a meta-analysis of normative functional neuroimaging studies. *Human brain mapping* **25**, 46-59 (2005).
72. Delis, D.C., Freeland, J., Kramer, J.H. & Kaplan, E. Integrating clinical assessment with cognitive neuroscience: construct validation of the California Verbal Learning Test. *Journal of consulting and clinical psychology* **56**, 123-130 (1988).
73. Loring, D.W., Martin, R.C., Meador, K.J. & Lee, G.P. Psychometric construction of the Rey-Osterrieth complex figure: Methodological considerations and interrater reliability. *Archives of Clinical Neuropsychology* **5**, 1-14 (1990).
74. Kaufman, J.N., Ross, T.J., Stein, E.A. & Garavan, H. Cingulate hypoactivity in cocaine users during a GO-NOGO task as revealed by event-related functional magnetic resonance imaging. *J Neurosci* **23**, 7839-7843 (2003).
75. Güth, W., Schmittberger, R. & Schwarze, B. An experimental analysis of ultimatum bargaining. *Journal of economic behavior & organization* **3**, 367-388 (1982).
76. Feeney, T., Hartwig, F.P. & Davies, N.M. How to use directed acyclic graphs: guide for clinical researchers. *BMJ* **388**, e078226 (2025).
77. Xu, Q.*, et al.* Distinct effects of early-stage and late-stage socioeconomic factors on brain and behavioral traits. *Nature Neuroscience* **28**, 676-687 (2025).
78. Van Dijk, K.R., Sabuncu, M.R. & Buckner, R.L. The influence of head motion on intrinsic functional connectivity MRI. *NeuroImage* **59**, 431-438 (2012).
79. Pereira, R.C., Abreu, P.H., Rodrigues, P.P. & Figueiredo, M.A.T. Imputation of data Missing Not at Random: Artificial generation and benchmark analysis. *Expert Systems with Applications* **249**(2024).
80. Li, J. & Ji, L. Adjusting multiple testing in multilocus analyses using the eigenvalues of a correlation matrix. *Heredity (Edinb)* **95**, 221-227 (2005).
81. Burnor, E.*, et al.* Association of Outdoor Ambient Fine Particulate Matter With Intracellular White Matter Microstructural Properties Among Children. *JAMA Netw Open* **4**, e2138300 (2021).
82. Jaiswal, C. & Singh, A.K. Particulate matter exposure and its consequences on hippocampal neurogenesis and cognitive function in experimental models. *Environ Pollut* **363**, 125275 (2024).
83. Wilker, E.H.*, et al.* Long-term exposure to fine particulate matter, residential proximity to major roads and measures of brain structure. *Stroke* **46**, 1161-1166 (2015).
84. Faherty, T., Raymond, J.E., McFiggans, G. & Pope, F.D. Acute particulate matter

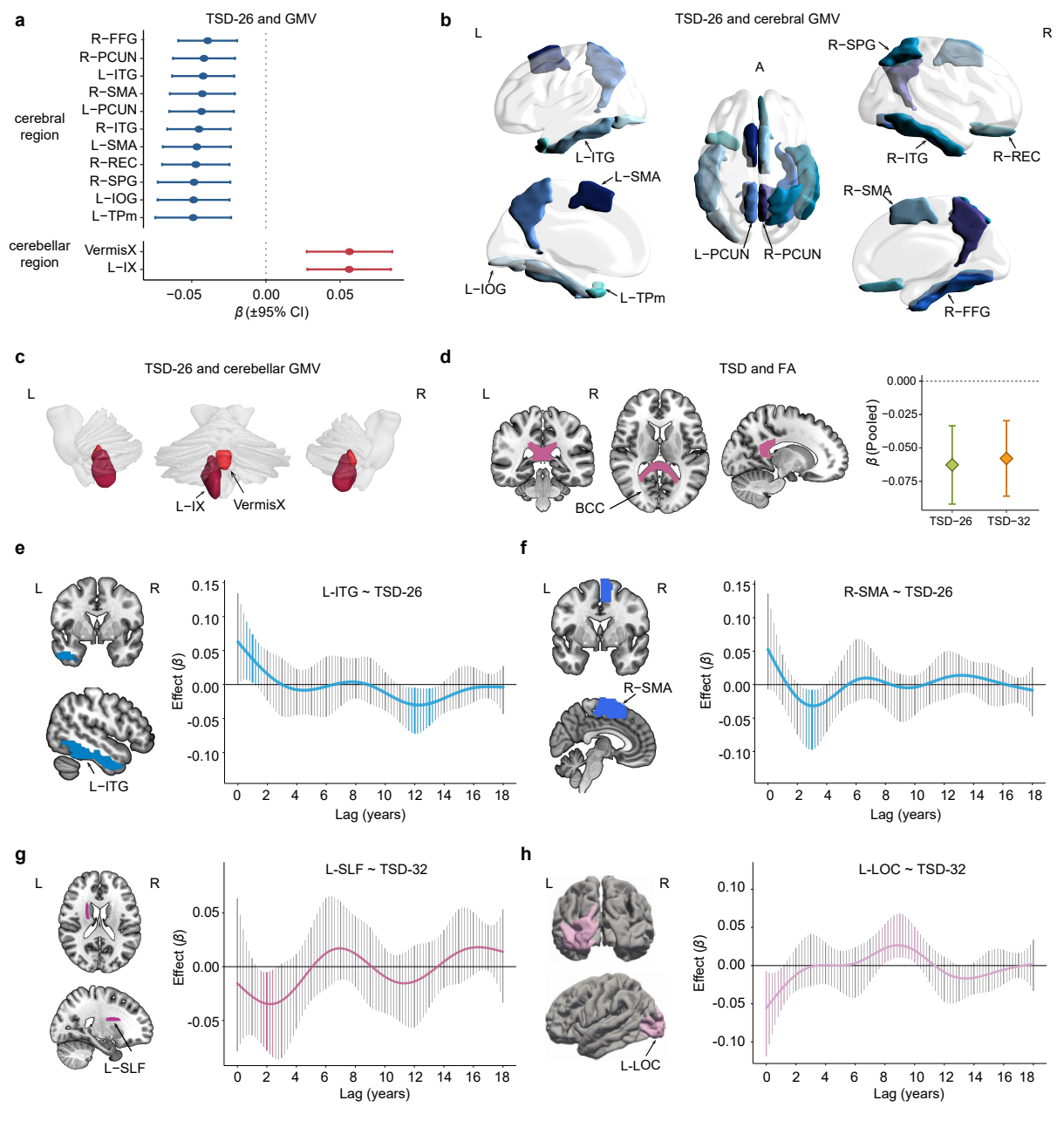
exposure diminishes executive cognitive functioning after four hours regardless of inhalation pathway. *Nat Commun* **16**, 1339 (2025).

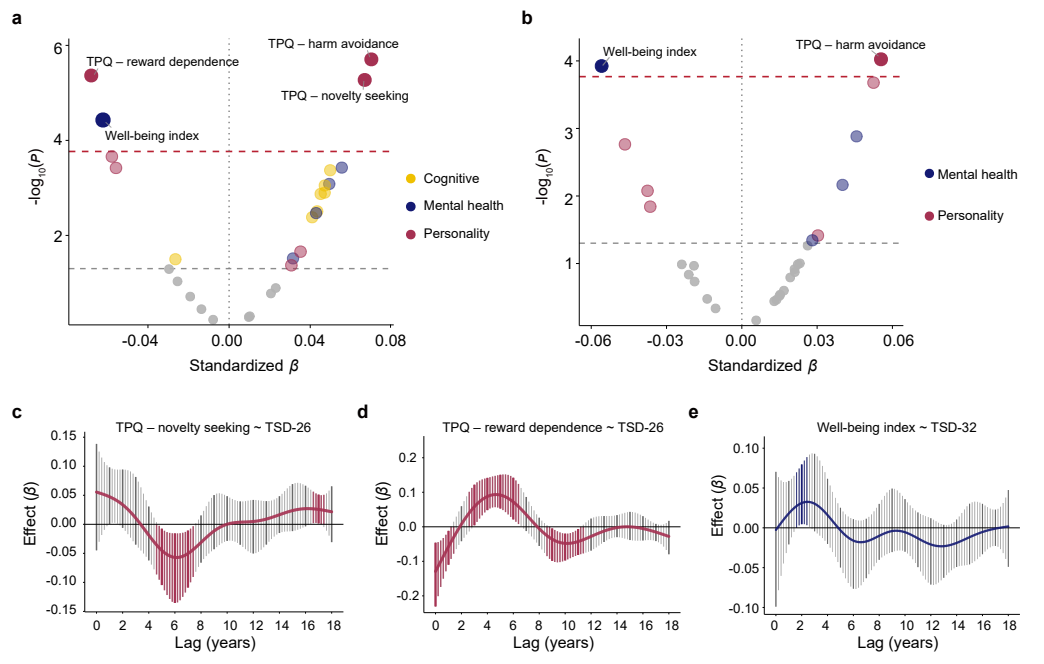
85. Jang, H.*, et al.* Combined effects of particulate and gaseous pollutants on Alzheimer's disease-related brain imaging markers and cognitive function. *Environ Pollut* **386**, 127260 (2025).

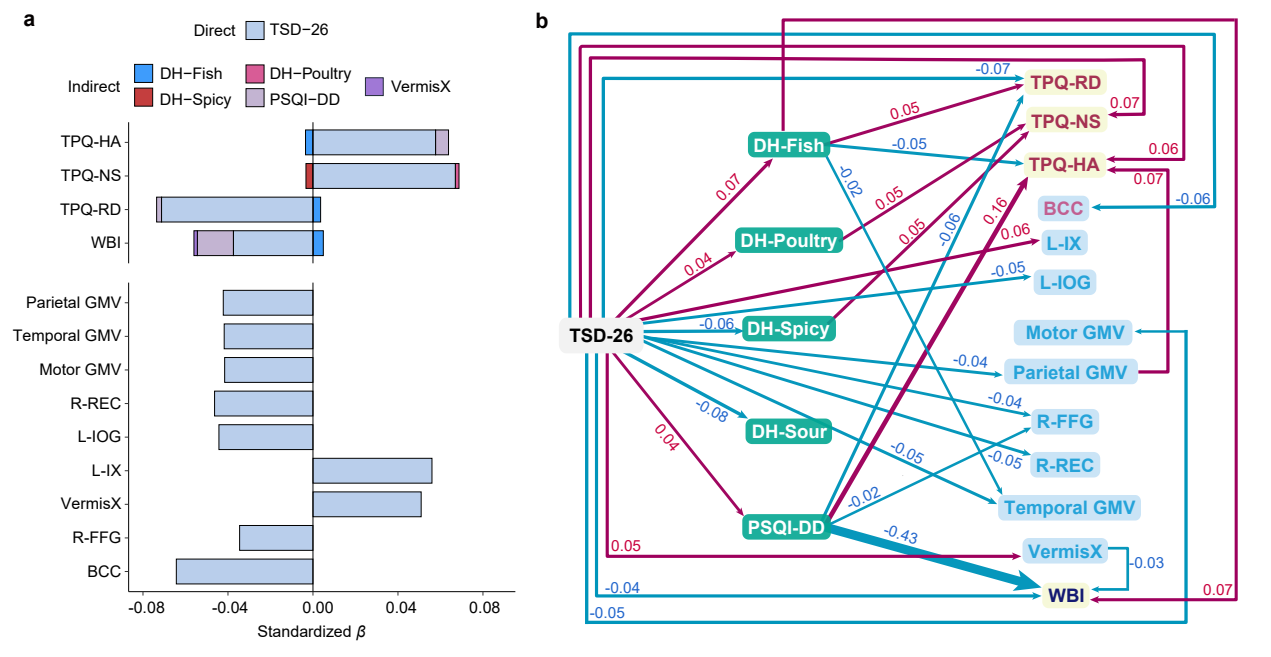
86. Cho, J.*, et al.* Long-Term Ambient Air Pollution Exposures and Brain Imaging Markers in Korean Adults: The Environmental Pollution-Induced Neurological EFfects (EPINEF) Study. *Environ Health Perspect* **128**, 117006 (2020).


Exposure assessment
a
Air temperature
Solar radiation
Humidity
Wind
Physiological model
Clothing model
UTCI (°C)
46
38
32
26
9
0
b
Number of participants
0
1–50
50–100
100–500
500–1,000
>1,000
CHIMGEN
Individual-level assignment
Timeline
Birth
Childhood
Adolescence
Early adulthood
1985
1993
1999
2003
2010
UTCI
Location
L1
L2
L3
L4
L5
c
UTCI > 32 °C
UTCI > 26 °C
Σ (hours above threshold)
Σ (Lifetime hours)
TSD-26 / TSD-32
Year
Hour
Analysis framework
d
Multivariable linear regression
Lifestyle measures
Dietary habits
Sleep
Mobile phone usage
Behavioral outcomes
Mental health
Personality
Cognitive function
Lifetime thermal stress
TSD-26
TSD-32
Brain imaging phenotypes
GMV
SA
CT
FA
BNFC
e
Distributed lag model
Behavior
Lifestyle
Neuroimaging
Effect
Birth
Childhood
Adolescence
f
Structural equation modeling
TSD-26
Lifestyle
Neuroimaging
Behavior
Direct and indirect pathways


a
Dietary habits – Taste preference: sour
Dietary habits – Taste preference: spicy
Dietary habits – Fish
PSQI – Daytime dysfunction
Dietary habits – Poultry
-log10(P)
Standardized β
b
Dietary habits – Taste preference: sour
Dietary habits – Taste preference: spicy
-log10(P)
Standardized β
c
TSD-26
Dietary habits – Fish
PSQI – Daytime dysfunction
Dietary habits – Taste preference: spicy
Dietary habits – Taste preference: sour
Ordinal logistic ln(OR)
Linear regression β
TSD-32
Dietary habits – Taste preference: spicy
Dietary habits – Taste preference: sour
Linear regression β
d
Dietary habits – Taste preference: sour ~ TSD-26
Dietary habits – Taste preference: spicy ~ TSD-26
Dietary habits – Poultry ~ TSD-26
PSQI – Daytime dysfunction ~ TSD-26
Effect (β)
Lag (years)


a
TSD-26 and GMV
cerebral region
R−FFG
R−PCUN
L−ITG
R−SMA
L−PCUN
R−ITG
L−SMA
R−REC
R−SPG
L−IOG
L−TPm
cerebellar region
VermisX
L−IX
−0.05
0.00
0.05
β (±95% CI)
b
TSD-26 and cerebral GMV
L
R
A
L−ITG
L−SMA
L−IOG
L−TPm
L−PCUN
R−PCUN
R−SPG
R−ITG
R−REC
R−SMA
R−FFG
c
TSD-26 and cerebellar GMV
L
R
L−IX
VermisX
d
TSD and FA
L
R
BCC
β (Pooled)
0.000
−0.025
−0.050
−0.075
TSD−26
TSD−32
e
L
R
L−ITG
L-ITG ~ TSD-26
Effect (β)
0.15
0.10
0.05
0.00
−0.05
−0.10
0 2 4 6 8 10 12 14 16 18
Lag (years)
f
L
R
R−SMA
R-SMA ~ TSD-26
Effect (β)
Lag (years)
g
L
R
L−SLF
L-SLF ~ TSD-32
Effect (β)
0.05
0.00
−0.05
Lag (years)
h
L
R
L-LOC
L-LOC ~ TSD-32
Effect (β)
0.10
0.05
0.00
−0.05
−0.10
Lag (years)


a
TPQ – harm avoidance
TPQ – reward dependence
TPQ – novelty seeking
Well-being index
-log10(P)
Standardized β
Cognitive
Mental health
Personality
b
Well-being index
TPQ – harm avoidance
-log10(P)
Standardized β
Mental health
Personality
c
TPQ – novelty seeking ~ TSD-26
Effect (β)
Lag (years)
d
TPQ – reward dependence ~ TSD-26
Effect (β)
Lag (years)
e
Well-being index ~ TSD-32
Effect (β)
Lag (years)


a
Direct
TSD−26
Indirect
DH−Fish
DH−Poultry
VermisX
DH−Spicy
PSQI−DD
TPQ-HA
TPQ-NS
TPQ-RD
WBI
Parietal GMV
Temporal GMV
Motor GMV
R-REC
L-IOG
L-IX
VermisX
R-FFG
BCC
-0.08
-0.04
0.00
0.04
0.08
Standardized β
b
TSD-26
DH-Fish
DH-Poultry
DH-Spicy
DH-Sour
PSQI-DD
TPQ-RD
TPQ-NS
TPQ-HA
BCC
L-IX
L-IOG
Motor GMV
Parietal GMV
R-FFG
R-REC
Temporal GMV
VermisX
WBI

Supplementary Files

This is a list of supplementary files associated with this preprint. Click to download.

- Supplementarytables260728.xlsx
- SupplementaryInformation260728.docx